DYNAMICS OF SLIDING AND LOADING BILAYER GRAPHENE

A THESIS SUBMITTED TO
THE GRADUATE SCHOOL OF ENGINEERING AND SCIENCE
OF BILKENT UNIVERSITY
IN PARTIAL FULFILLMENT OF THE REQUIREMENTS FOR
THE DEGREE OF
MASTER OF SCIENCE
IN
PHYSICS

By
Benjamin Edun
September 2022

Dynamics of Sliding and Loading Bilayer Graphene
By Benjamin Edun
September 2022

We certify that we have read this thesis and that in our opinion it is fully adequate, in scope and in quality, as a thesis for the degree of Master of Science.

Oğuz Gülseren(Advisor)

Ceren Sibel Sayin

Emre Taşci

Approved for the Graduate School of Engineering and Science:

Orhan Arıkan
Director of the Graduate School

ABSTRACT

DYNAMICS OF SLIDING AND LOADING BILAYER GRAPHENE

Benjamin Edun
M.S. in PHYSICS
Advisor: Oğuz Gülseren
September 2022

Sliding and loading bilayer graphene is investigated using the Tight Binding method. We develop interaction-distance dependent tight binding parameter functions to allow for the calculation of band structure for different interacting distances. We investigate the band structures of sliding graphene and loading bilayer graphene, in which case the latter consists of varying interlayer distances between monolayers. We show that based on developed parameter models, band splittings can be seen to emerge in the band structures, which follow different patterns for different sliding directions. As expected we confirm that for varying vertical interlayer distances, monolayer graphene band structure is the limit for both AA and AB stacking configurations. By applying a quadratic energy model to the curvature of the band structures in the vicinity of the K-point for AB stacking configuration we predict the effective mass of electrons and holes in bilayer graphene, and electrons in monolayer graphene. We also show the pattern of change of effective mass with respect to changing interlayer distance, and try to investigate where our prescribed quadractic energy model breaks down, as we approach the limit of the monolayer band structure.

Keywords: Monolayer Graphene, Bilayer Graphene, Sliding Bilayer Graphene, Loading Bilayer Graphene, Tight Binding Model, Tight Binding Parameters, Tight Binding Parameter Functions, Conduction Band, Valence band, Band Gap, Band splitting, Effective Mass, Second Nearest Neighbour (2NN), Fourth Nearest Neighbour (4NN), Brillouin Zone (BZ).

ÖZET

KAYDIRMA VE YÜKLEME ALTINDA ÇİFT KATMANLI GRAFENİN DİNAMİKLERİ

Benjamin Edun
Fizik, Yüksek Lisans
Bu Tez Çalışmasında Danışmanı: Oğuz Gülseren
Eylül 2022

Iki katmanlı grafenin kayması ve yüklenmesi, Sıkı Bağlama yöntemi kullanılarak incelenmiştir. Farklı etkileşim mesafeleri için bant yapısının hesaplanmasına izin vermek için etkileşim mesafesine bağlı sıkı bağlama parametre fonksiyonları geliştirildi. Kayan grafenin bant yapılarını ve çift katmanlı grafen yükleme araştırıldı, bu durumda ikincisi tek katmanlar arasında değişen katmanlar arası mesafelerden oluşmaktadır. Geliştirilen parametre modellerine dayanarak, farklı kayma yönleri için farklı desenler izleyen bant yapılarında bant açılmalarının ortaya çıktığını görmekteyiz. Beklendiği gibi, değişen dikey ara katman mesafeleri için, tek katmanlı grafen bant yapısının hem AA hem de AB istifleme konfigürasyonları için sınır olduğunu teyit edilmiştir. AB istifleme konfigürasyonu için K noktasının yakınındaki bant yapılarının eğriliğine ikinci dereceden bir enerji modeli uygulayarak, çift katmanlı grafen içindeki elektronların ve boşlukların ve tek katmanlı grafen içindeki elektronların etkin kütlesini hesaplandı. Ayrıca, değişen ara katman mesafesine göre etkin kütlenin değişim modelini gösterildi ve tek katmanlı bant yapısının sınırına yaklaşırken, öngörülen kuadratik enerji modelimizin nerede bozulduğunu araştırıldı.

Anahtar sözcükler: Tek Katmanlı Grafen, Çift Katmanlı Grafen, Kayan Çift Katmanlı Grafen, Çift Katmanlı Grafen Yükleme, Sıkı Bağlama Modeli, Sıkı Bağlama Parametreleri, Sıkı Bağlama parametresi Fonksiyonları, İletim Bandı, Değerlilik bandı, Bant Boşluğu, Etkin, İkinci En Yakın Komşu(2NN), Dördüncü En Yakın Komşu(4NN), Brillouin Bölgesi (BZ) .

Acknowledgement

"This is the day which the lord hath made, we'll rejoice and be glad in it"

I thank God Almighty for the strength over this period. I thank my supervisor, Professor Oğuz Gülseren for his support throughout my research, in the lead up to this thesis, and especially for providing encouragement much earlier when i was constantly running into roadblocks, and his insights on how to resolve my research frustrations early on. I am grateful to my colleagues. Certainly, however small, they have contributed to the wealth of knowledge i have today. I would like to thank my friends including Zacharia, Arma, Abel, Kamil, Kayode, Aliyu, Charlie among many others, mostly from the African community for providing moral support, at different times, and making me feel at home. I will not forget the occasional get-together organized by you guys, where we cooked and ate together. I will not forget my footballing friends too. Health is wealth. I am grateful to friends from yesteryears that have remained in contact, and have been supportive at different times.
Finally, i thank my family for their prayers and immeasurable support.

On this note, i dedicate this to the Edunjobi family

Contents

List of Figures

List of Tables

Chapter 1

Introduction

1.1 Motivation

The band structure of graphite and therefore multilayered graphene has been well treated in Density Functional Theory-based methods and the Tight-Binding method[1, 2, 3]. However most of the discussions have been limited to the electronic band structures of AA and AB bilayer stackings, in which case the tight-binding parameters required have been provided. For the most part, with respect to the bands most affected, researchers have mostly focused on the lower lying bands, that's the bands that result from p_z orbital interactions for atoms in and out of plane. A comprehensive review on the more extensive graphite was made by [4], in which case the values of the appropriate Slonczewski-Weiss-McClure(SWMCc) tight binding parameters as determined experimentally were discussed. Further down the line, [5] reported SWMCc tight binding parameters slightly different from the review by [4], obtained by using different experimental methods. I would like to also mention that some work has been done on friction in single and multilayered graphene [6], which is part part of our motivation for investigating the electronic band structure changes in sliding and loading bilayer graphene, which can be associated with the lateral force and normal force in bilayer graphene respectively. For the most part though, extensive discussions

on how the band structure of bilayer graphene varies for a bilayer in which the relative positions of the chosen bases atoms in the monolayers are changing in directions parallel/perpendicular to haxagonal axis have been scarce, especially because for any of these cases the relative distance between the interacting basis atoms change, thus interaction potentials change, therefore the tight-binding parameters have to be re-calculated, which in fact is usually the problem with respect to parameter based band-structure calculations. Our work is an attempt at providing a reasonable scaling law, that will enable us determine the tight binding parameters at arbitrary interacting distances, at least up to a distance, and thus be able to follow the change in the band structure as the monolayers slide across or pull apart in a direction perpendicular to the hexagonal axis.

1.2 Multilayer Graphene

From Wallace [7] to DiVincenzo and Mele [8], there have been several discussions of monolayer and multilayered graphene much before the isolation of a few layer sheet(s) of graphene were realized by Geim and Novoselov in their groundbreaking work[9] in 2004. The interesting thing about graphene and its nanostructures is the variation of their properties, be it electronic, magnetic, optical and mechanical as limitations to shape and size are applied, as manifested in tunable band gaps in bilayer graphene [10], nanoribbons [11, 12, 13, 14], carbon nanotubes [15, 16], and in magic angle graphene superlattices [17], in which superconduction was discovered.This points to an allowance for engineering of these nanostructures into devices that posess specific desirable properties.

1.3 Structure of Thesis

The rest of this is organized into the following parts. In chapter 2 we discuss the tight binding model extensively. In chapter 3, sliding bilayer-upper monolayer shifting(in it's horizontal plane) relative to another. In chapter 4 we discuss

loading bilayer graphene (changing separation distance) and the band splittings that result. In chapter 5 we investigate the effective mass of electrons and holes in loading bilayer graphene.

Chapter 2

Tight Binding Model

The Tight Binding approximation, also referred to as Linear Combination of Atomic Orbitals (LCAO) is the simplest method for computing electronic band structure [18]. It assumes block orbitals can be constructed from the atomic wavefunctions similar to those constituting the atoms, so that the overlap of atomic orbitals is enough to account for the correction to the picture of isolated atoms. The more the atomic orbitals, the more the description looks reasonable. As can be concluded from "tight binding', it assumes the wavefunctions are tightly bound to the atoms. So given a set of atomic wavefunctions $\psi_l(r - R_j)$, where l represents the angular momentum character s, d, f e.t.c, and j, the position of atoms specifying the atomic orbitals, we can generate bloch theorem obedient normalized atomic wavefunctions,

$$|\varphi_{klj}(r)\rangle = \frac{1}{\sqrt{N}} \sum_{j=1}^{N} e^{i\mathbf{k}\cdot\mathbf{R_j}} \phi_l(\mathbf{r} - \mathbf{R_j}), \tag{2.1}$$

We then express the crystal wavefunctions as linear combinations of these bloch-theorem-obedient atomic wave functions, so that the crystal wave function,

$$|\psi_k(r)\rangle = \sum_l c_{klj} \varphi_{klj}(r), \tag{2.2}$$

The one-electron hamiltonian eigenvalue problem

$$\mathbf{H} \left|\psi_k(r)\right\rangle = \epsilon_k \left|\psi_k(r)\right\rangle, \tag{2.3}$$

can the be written as,

$$\mathbf{H}\left|\psi_k(r)\right\rangle = \epsilon_k \sum_l c_{klj}\varphi_{klj}(r), \tag{2.4}$$

and

$$\mathbf{H}\left|\psi_k(r)\right\rangle = \sum_l \mathbf{H}c_{klj}\left|\varphi_{klj}(r)\right\rangle, \tag{2.5}$$

Comparing Eqs. 2.4 and 2.5 and taking inner product with $\langle\varphi_{kl'j'}(r)|$, we obtain the secular equation,

$$\sum_l \Big[\big\langle\varphi_{kl'j'}(r)|\mathbf{H}|\varphi_{klj}(r)\big\rangle - \epsilon_k\big\langle\varphi_{kl'j'}(r)|\varphi_{klj}(r)\big\rangle\Big]c_{klj} = 0, \tag{2.6}$$

which requires that,

$$|H - ES| = 0, \tag{2.7}$$

where H and S are the corresponding hamiltonian and overlap matrices in reference to Eq. 2.6, and E the energy eigen-values.
The matrix overlap elements in Eq. 2.6,

$$\big\langle\varphi_{kl'j'}(r)|\varphi_{klj}(r)\big\rangle = \frac{1}{N}\sum_{\mathbf{j}=\mathbf{1}}^{N}\sum_{\mathbf{j'}=\mathbf{1}}^{N} e^{i\mathbf{k}\cdot(\mathbf{R_j}-\mathbf{R_{j'}})}\big\langle\phi_{l'}(\mathbf{r}-\mathbf{R_{j'}})|\phi_l(\mathbf{r}-\mathbf{R_j})\big\rangle \tag{2.8}$$

and similarly the hamiltonian elements,

$$\big\langle\varphi_{kl'j'}(r)|\mathbf{H}|\varphi_{klj}(r)\big\rangle = \frac{1}{N}\sum_{\mathbf{j}=\mathbf{1}}^{N}\sum_{\mathbf{j'}=\mathbf{1}}^{N} e^{i\mathbf{k}\cdot(\mathbf{R_j}-\mathbf{R_{j'}})}\big\langle\phi_{l'}(\mathbf{r}-\mathbf{R_{j'}})|\mathbf{H}|\phi_l(\mathbf{r}-\mathbf{R_j})\big\rangle \tag{2.9}$$

2.1 Interaction of Orbitals

Fig. 2.1 shows the interaction between the s orbitals, and Fig. 2.2a, the interaction between the s and p orbitals.
For an arbitrarily oriented orbital $|p\rangle$ initially subtending an angle ϕ rotated through an angle θ, counterclockwise,

$$|p\rangle = \cos\phi\cos\theta\,|p_{x\prime}\rangle - \sin\phi\sin\theta\,|p_{y\prime}\rangle + \sin\phi\cos\theta\,|p_{x\prime}\rangle + \cos\phi\sin\theta\,|p_{y\prime}\rangle\,, \tag{2.10}$$

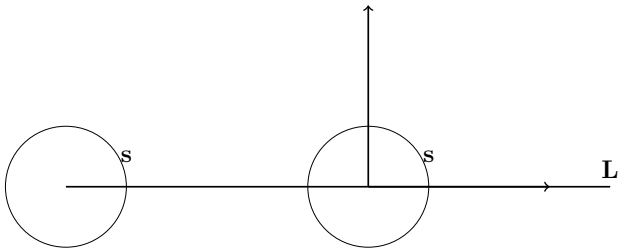

Figure 2.1: Interaction between s and s orbitals

where θ subsumes ϕ so that $\phi = 0$,

$$|p\rangle = \cos\theta\,|p_{x\prime}\rangle + \sin\theta\,|p_{y\prime}\rangle\,, \tag{2.11}$$

Thus,

$$\langle s|p\rangle = \cos\theta\,\langle s|p_{x\prime}\rangle + \sin\theta\,\langle s|p_{y\prime}\rangle = \cos\theta\,\langle s|p_{x\prime}\rangle \tag{2.12}$$

For Fig. 2.2b,

$$|p_1\rangle = \cos\theta_1\,|p_{x\prime}\rangle + \sin\theta_1\,|p_{y\prime}\rangle \tag{2.13}$$

$$|p_2\rangle = \cos\theta_2\,|p_{x\prime}\rangle + \sin\theta_2\,|p_{y\prime}\rangle\,, \tag{2.14}$$

and using orthogonality,

$$\langle p_1|p_2\rangle = \cos\theta_1\cos\theta_2\,\langle p_{x\prime}|p_{x\prime}\rangle + \sin\theta_2\sin\theta_2\,\langle p_{y\prime}|p_{y\prime}\rangle\,, \tag{2.15}$$

where $|p_{x\prime}\rangle$ is always parallel to the line joining the centers of the interacting orbitals.

Similarly for the hamiltonian interactions,

$$\langle s|\mathbf{H}|p\rangle = \cos\theta\,\langle s|\mathbf{H}|p_{x\prime}\rangle \tag{2.16}$$

$$\langle p_1|\mathbf{H}|p_2\rangle = \cos\theta_1\cos\theta_2\,\langle p_{x\prime}|\mathbf{H}|p_{x\prime}\rangle + \sin\theta_2\sin\theta_2\,\langle p_{y\prime}|\mathbf{H}|p_{y\prime}\rangle\,, \tag{2.17}$$

Eq. 2.16 can be rewritten as

$$\langle s|\mathbf{H}|p\rangle = \pm|H_{sp\sigma}|\cos(180-\theta), \tag{2.18}$$

so that we only focus on the angle between the interacting lobe and the line **L**, in which the sign is positive if the interacting half is the positive lobe and negative if the interacting half is the negative lobe.

Eq. 2.17 can also be rewritten as,

$$\langle p_1|\mathbf{H}|p_2\rangle = \pm|H_{pp\sigma}|\cos\theta_1\cos(180-\theta_2) \pm |H_{pp\pi}|\sin\theta_1\sin(180-\theta_2), \tag{2.19}$$

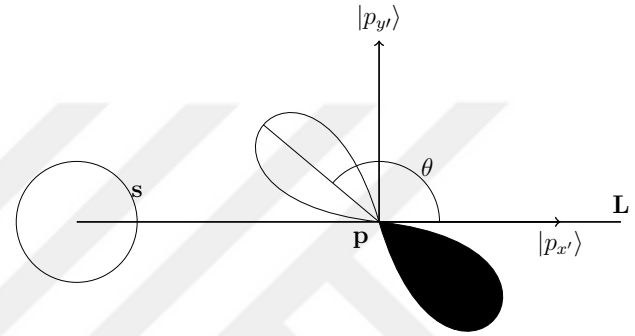

(a)

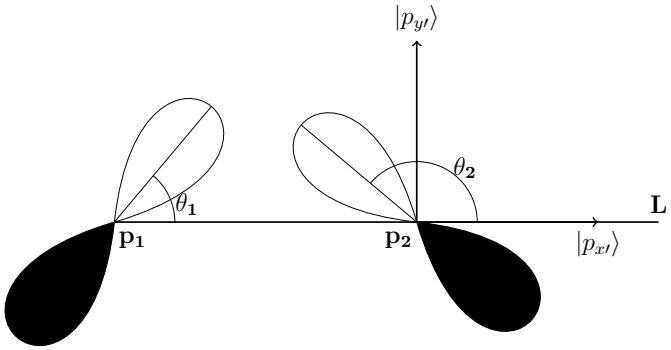

(b)

Figure 2.2: (a) Interaction between s and p orbitals (b) Interactions between p and p orbitals

for the same reason as eq. 2.20, but in which case this time the signs depend on if the interacting lobes are attractive or repulsive. The sign is positive if the interacting lobes are neither both positive or negative, and negative if the interacting lobes are both positive or negative.

2.2 Monolayer Graphene

Given an origin located at the basis atom **A**,

$$\begin{aligned}\delta_1 &= \left(\frac{a}{\sqrt{3}}, 0\right)\\ \delta_2 &= \left(-\frac{a}{2\sqrt{3}}, \frac{a}{2}\right)\\ \delta_3 &= \left(-\frac{a}{2\sqrt{3}}, -\frac{a}{2}\right)\end{aligned} \tag{2.20}$$

are the first nearest neighbor interaction vectors, where $a = 2.46\,\text{Å}$, is the lattice parameter. Considering the two sublattices **A** and **B** in monolayer graphene, and in reference to Eq. 2.9 we have the hamiltonian and overlap block matrices,

$$H = \begin{bmatrix} H_{AA} & H_{AB} \\ H_{AB}^* & H_{BB} \end{bmatrix} \tag{2.21}$$

and

$$S = \begin{bmatrix} S_{AA} & S_{AB} \\ S_{AB}^* & S_{BB} \end{bmatrix}, \tag{2.22}$$

respectively, where

$$\mathbf{H_{AA}} = \begin{bmatrix} \langle s_A|H|s_{A'}\rangle & \langle s_A|H|p_{x_{A'}}\rangle & \langle s_A|H|p_{y_{A'}}\rangle & \langle s_A|H|p_{z_{A'}}\rangle \\ \langle p_{x_A}|H|s_{A'}\rangle & \langle p_{x_A}|H|p_{x_{A'}}\rangle & \langle p_{x_A}|H|p_{y_{A'}}\rangle & \langle p_{x_A}|H|p_{z_{A'}}\rangle \\ \langle p_{y_A}|H|p_{s_{A'}}\rangle & \langle p_{y_A}|H|p_{x_{A'}}\rangle & \langle p_{y_A}|H|p_{y_{A'}}\rangle & \langle p_{y_A}|H|p_{z_{A'}}\rangle \\ \langle p_{z_A}|H|p_{s_{A'}}\rangle & \langle p_{z_A}|H|p_{x_{A'}}\rangle & \langle p_{z_A}|H|p_{y_{A'}}\rangle & \langle p_{z_A}|H|p_{z_{A'}}\rangle \end{bmatrix}, \tag{2.23}$$

$$\mathbf{S_{AA}} = \begin{bmatrix} \langle s_A|s_{A'}\rangle & \langle s_A|p_{x_{A'}}\rangle & \langle s_A|p_{y_{A'}}\rangle & \langle s_A|p_{z_{A'}}\rangle \\ \langle p_{x_A}|s_{A'}\rangle & \langle p_{x_A}|p_{x_{A'}}\rangle & \langle p_{x_A}|p_{y_{A'}}\rangle & \langle p_{x_A}|p_{z_{A'}}\rangle \\ \langle p_{y_A}|p_{s_{A'}}\rangle & \langle p_{y_A}|p_{x_{A'}}\rangle & \langle p_{y_A}|p_{y_{A'}}\rangle & \langle p_{y_A}|p_{z_{A'}}\rangle \\ \langle p_{z_A}|p_{s_{A'}}\rangle & \langle p_{z_A}|p_{x_{A'}}\rangle & \langle p_{z_A}|p_{y_{A'}}\rangle & \langle p_{z_A}|p_{z_{A'}}\rangle \end{bmatrix}, \tag{2.24}$$

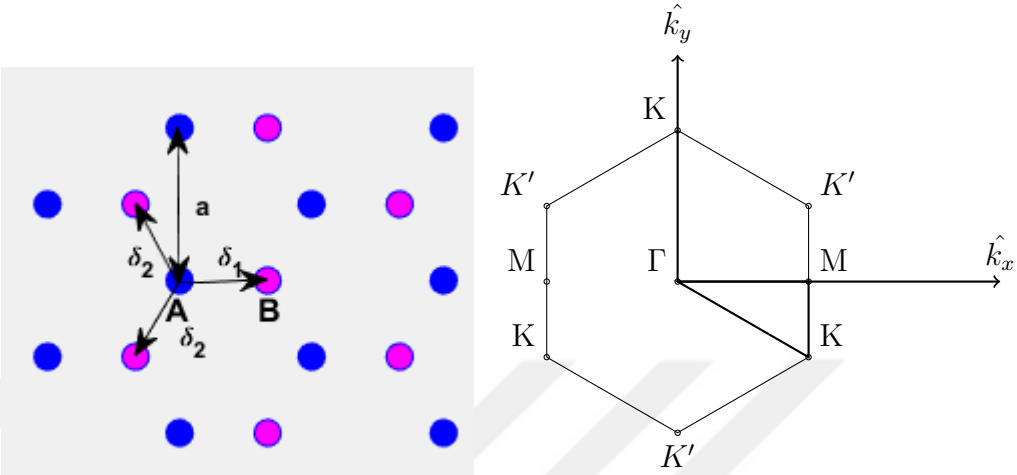

(a) (b)

Figure 2.3: (a) Monolayer Lattice. (b) First Brillouin Zone

in which case A' includes all atoms in A, and the distinction only indicating an interaction between orbitals of two atoms in the same sub lattice. $\mathbf{H_{BB}}$ is simply $\mathbf{H_{AA}}$ with A and A' replaced with B and B' respectively.
For interactions up to First Nearest Neighbours(1NN),

$$\mathbf{H_{AA}} = \mathbf{H_{BB}} = \begin{bmatrix} E_{2s} & 0 & 0 & 0 \\ 0 & E_{2p} & 0 & 0 \\ 0 & 0 & E_{2p} & 0 \\ 0 & 0 & 0 & E_{2p} \end{bmatrix}, \tag{2.25}$$

$$\mathbf{S_{AA}} = \mathbf{S_{BB}} = \begin{bmatrix} 1 & 0 & 0 & 0 \\ 0 & 1 & 0 & 0 \\ 0 & 0 & 1 & 0 \\ 0 & 0 & 0 & 1 \end{bmatrix}, \tag{2.26}$$

$$\mathbf{H_{AB}} = \begin{bmatrix} \langle s_B|H|s_A\rangle & \langle p_{x_B}|H|s_A\rangle & \langle p_{y_B}|H|s_A\rangle & \langle p_{z_B}|H|s_A\rangle \\ \langle s_B|H|p_{x_A}\rangle & \langle p_{x_B}|H|p_{x_A}\rangle & \langle p_{y_B}|H|p_{x_A}\rangle & \langle p_{z_B}|H|p_{x_A}\rangle \\ \langle p_{s_B}|H|p_{y_A}\rangle & \langle p_{x_B}|H|p_{y_A}\rangle & \langle p_{y_B}|H|p_{y_A}\rangle & \langle p_{y_A}|H|p_{z_B}\rangle \\ \langle p_{s_B}|H|p_{z_A}\rangle & \langle p_{x_B}|H|p_{z_A}\rangle & \langle p_{y_B}|H|p_{z_A}\rangle & \langle p_{z_B}|H|p_{z_A}\rangle \end{bmatrix}, \tag{2.27}$$

$$\mathbf{S_{AB}} = \begin{bmatrix} \langle s_B|s_A\rangle & \langle p_{x_B}|s_A\rangle & \langle p_{y_B}|s_A\rangle & \langle p_{z_B}|s_A\rangle \\ \langle s_B|p_{x_A}\rangle & \langle p_{x_B}|p_{x_A}\rangle & \langle p_{y_B}|p_{x_A}\rangle & \langle p_{z_B}|p_{x_A}\rangle \\ \langle p_{s_B}|p_{y_A}\rangle & \langle p_{x_B}|p_{y_A}\rangle & \langle p_{y_B}|p_{y_A}\rangle & \langle p_{y_A}|p_{z_B}\rangle \\ \langle p_{s_B}|p_{z_A}\rangle & \langle p_{x_B}|p_{z_A}\rangle & \langle p_{y_B}|p_{z_A}\rangle & \langle p_{z_B}|p_{z_A}\rangle \end{bmatrix}, \tag{2.28}$$

$$\begin{aligned} H_{11} = \langle s_A|\mathbf{H}|s_B\rangle &= \sum_{\delta} \langle s(r)|\mathbf{H}|s(r-R_{AB}\rangle\, e^{ik\cdot R_{AB}} \\ &= H_{ss\sigma}\cdot\left(e^{-i\frac{k_x a}{\sqrt{3}}} + 2e^{i\frac{k_x a}{2\sqrt{3}}}\cos\left(\frac{k_y a}{2}\right)\right) \end{aligned} \tag{2.29}$$

$$\begin{aligned} H_{15} = \langle p_{x_B}|\mathbf{H}|s_A\rangle &= \sum_{\delta} \langle s(r)|\mathbf{H}|p(r-R_{AB})\rangle\, e^{ik\cdot R_{AB}} \\ &= |H_{sp\sigma}|\cdot\left(-e^{-i\frac{k_x a}{\sqrt{3}}} + e^{i\frac{k_x a}{2\sqrt{3}}}\cos\left(\frac{k_y a}{2}\right)\right) \end{aligned} \tag{2.30}$$

$$\begin{aligned} H_{16} = \langle p_{y_B}|\mathbf{H}|s_A\rangle &= \sum_{\delta} \langle s(r)|\mathbf{H}|p(r-R_{AB})\rangle\, e^{ik\cdot R_{AB}} \\ &= |H_{sp\sigma}|\cdot\sqrt{3}\cdot e^{i\frac{k_x a}{2\sqrt{3}}}\sin\left(\frac{k_y a}{2}\right) i \end{aligned} \tag{2.31}$$

$$\begin{aligned} H_{25} = \langle p_{x_B}|\mathbf{H}|p_{x_A}\rangle &= \sum_{\delta} \langle p_1(r)|\mathbf{H}|p_2(r-R_{AB})\rangle\, e^{ik\cdot R_{AB}} \\ &= |H_{pp\sigma}|\cdot e^{-i\frac{k_x a}{\sqrt{3}}} + \frac{1}{4}\left(|H_{pp\sigma} + 3|H_{pp\pi}|\right)\cdot e^{i\frac{k_x a}{2\sqrt{3}}}\cos\left(\frac{k_y a}{2}\right) \end{aligned} \tag{2.32}$$

$$\begin{aligned} H_{36} = \langle p_{y_B}|\mathbf{H}|p_{y_A}\rangle &= \sum_{\delta} \langle p_1(r)|\mathbf{H}|p_2(r-R_{AB})\rangle\, e^{ik\cdot R_{AB}} \\ &= |H_{pp\pi}|\cdot e^{-i\frac{k_x a}{\sqrt{3}}} + \frac{1}{4}\left(3|H_{pp\sigma} + |H_{pp\pi}|\right)\cdot e^{i\frac{k_x a}{2\sqrt{3}}}\cos\left(\frac{k_y a}{2}\right) \end{aligned} \tag{2.33}$$

$$\begin{aligned} H_{26} = \langle p_{y_B}|\mathbf{H}|p_{x_A}\rangle &= \sum_{\delta} \langle s(r)|\mathbf{H}|p(r-R_{AB})\rangle\, e^{ik\cdot R_{AB}} \\ &= \frac{\sqrt{3}}{4}\left(3|H_{pp\sigma} + |H_{pp\pi}|\right)\sqrt{3}e^{i\frac{k_x a}{2\sqrt{3}}}\sin\left(\frac{k_y a}{2}\right) i \end{aligned} \tag{2.34}$$

$$H_{48} = \langle p_{z_B}|\mathbf{H}|p_{z_A}\rangle = \sum_{\delta} \langle s(r)|\mathbf{H}|s(r-R_{AB}\rangle\, e^{ik\cdot R_{AB}}$$
$$= H_{pp\pi} \cdot \left(e^{-i\frac{k_x a}{\sqrt{3}}} + 2e^{i\frac{k_x a}{2\sqrt{3}}} \cos\left(\frac{k_y a}{2}\right)\right) \tag{2.35}$$

$$H_{25} = -H_{16} \implies \langle s_B|\mathbf{H}|p_{x_A}\rangle = -\langle p_{x_B}|H|s_A\rangle$$
$$H_{17} = -H_{35} \implies \langle s_B|H|p_{y_A}\rangle = -\langle p_{y_B}|H|s_A\rangle$$
$$H_{27} = H_{36} \implies \langle p_{x_B}|H|p_{y_A}\rangle = \langle p_{y_B}|H|p_{x_A}\rangle \tag{2.36}$$

Similarly,

$$S_{15} = |S_{sp\sigma}| \cdot \left(-e^{-i\frac{k_x a}{\sqrt{3}}} + e^{i\frac{k_x a}{2\sqrt{3}}} \cos\left(\frac{k_y a}{2}\right)\right) \tag{2.37}$$

$$S_{16} = |S_{sp\sigma}| \cdot \sqrt{3} \cdot e^{i\frac{k_x a}{2\sqrt{3}}} \sin\left(\frac{k_y a}{2}\right) i \tag{2.38}$$

$$S_{25} = |S_{pp\sigma}| \cdot e^{-i\frac{k_x a}{\sqrt{3}}} + \frac{1}{4}\left(|S_{pp\sigma} + 3|H_{pp\pi}|\right) \cdot e^{i\frac{k_x a}{2\sqrt{3}}} \cos\left(\frac{k_y a}{2}\right) \tag{2.39}$$

$$S_{26} = \frac{\sqrt{3}}{4}\left(3|H_{pp\sigma} + |S_{pp\pi}|\right)\sqrt{3} e^{i\frac{k_x a}{2\sqrt{3}}} \sin\left(\frac{k_y a}{2}\right) i \tag{2.40}$$

$$S_{36} = |S_{pp\pi}| \cdot e^{-i\frac{k_x a}{\sqrt{3}}} + \frac{1}{4}\left(3|S_{pp\sigma} + |H_{pp\pi}|\right) \cdot e^{i\frac{k_x a}{2\sqrt{3}}} \cos\left(\frac{k_y a}{2}\right) \tag{2.41}$$

$$S_{48} = H_{pp\pi} \cdot \left(e^{-i\frac{k_x a}{\sqrt{3}}} + 2e^{i\frac{k_x a}{2\sqrt{3}}} \cos\left(\frac{k_y a}{2}\right)\right) \tag{2.42}$$

where $R_{AB} = R_A - R_B$

Element-wise,

$$H = \begin{bmatrix} H_{11} & H_{12} & H_{13} & H_{14} & H_{15} & H_{16} & H_{17} & H_{18} \\ H_{21} & H_{22} & H_{23} & H_{24} & H_{25} & H_{26} & H_{27} & H_{28} \\ H_{31} & H_{32} & H_{33} & H_{34} & H_{35} & H_{36} & H_{37} & H_{38} \\ H_{41} & H_{42} & H_{43} & H_{44} & H_{45} & H_{46} & H_{47} & H_{48} \\ H_{51} & H_{52} & H_{53} & H_{54} & H_{55} & H_{56} & H_{57} & H_{58} \\ H_{61} & H_{62} & H_{63} & H_{64} & H_{65} & H_{66} & H_{67} & H_{68} \\ H_{71} & H_{72} & H_{73} & H_{74} & H_{75} & H_{76} & H_{77} & H_{78} \\ H_{81} & H_{82} & H_{83} & H_{84} & H_{85} & H_{86} & H_{87} & H_{88} \end{bmatrix} \tag{2.43}$$

$$S = \begin{bmatrix} S_{11} & S_{12} & S_{13} & S_{14} & S_{15} & S_{16} & S_{17} & S_{18} \\ S_{21} & S_{22} & S_{23} & S_{24} & S_{25} & S_{26} & S_{27} & S_{28} \\ S_{31} & S_{32} & S_{33} & S_{34} & S_{35} & S_{36} & S_{37} & S_{38} \\ S_{41} & S_{42} & S_{43} & S_{44} & S_{45} & S_{46} & S_{47} & S_{48} \\ S_{51} & S_{52} & S_{53} & S_{54} & S_{55} & S_{56} & S_{57} & S_{58} \\ S_{61} & S_{62} & S_{63} & S_{64} & S_{65} & S_{66} & S_{67} & S_{68} \\ S_{71} & S_{72} & S_{73} & S_{74} & S_{75} & S_{76} & S_{77} & S_{78} \\ S_{81} & S_{82} & S_{83} & S_{84} & S_{85} & S_{86} & S_{87} & S_{88} \end{bmatrix} \tag{2.44}$$

$$H^*_{AB} = \begin{bmatrix} H_{51} & H_{52} & H_{53} & H_{54} \\ H_{61} & H_{62} & H_{63} & H_{64} \\ H_{71} & H_{72} & H_{73} & H_{74} \\ H_{81} & H_{82} & H_{83} & H_{84} \end{bmatrix} = \begin{bmatrix} H^*_{11} & H^*_{12} & H^*_{13} & H^*_{14} \\ H^*_{21} & H^*_{22} & H^*_{23} & H^*_{24} \\ H^*_{31} & H_{32} & H^*_{33} & H^*_{34} \\ H^*_{41} & H^*_{42} & H^*_{43} & H^*_{44} \end{bmatrix} \tag{2.45}$$

Using Eq. 2.7, for the following table of tight binding parameters [19], which are determined by fitting the model to the electronic band structure from experimental or the more accurate DFT, at high-symmetry points. We draw the band structure along the $\Gamma - K - M - \Gamma$ directions, localized on the edges of a triangle, where

$$\Gamma = (0,0)\,, K = \left(\frac{2\pi}{\sqrt{3}a}, -\frac{2\pi}{3a}\right), M = \left(\frac{2\pi}{\sqrt{3}a}, 0\right) \tag{2.46}$$

Parameter	value(eV)
ϵ_{2s}	-8.70
ϵ_{2p}	0.00
$H_{ss\sigma}$	-6.70
$H_{sp\sigma}$	5.50
$H_{pp\sigma}$	5.10
$H_{pp\pi}$	-3.10
$S_{ss\sigma}$	0.20
$S_{sp\sigma}$	-0.10
$S_{pp\sigma}$	-0.15
$S_{pp\pi}$	0.12

Table 2.1: Table of Tight Binding Parameters (Monolayer Graphene)

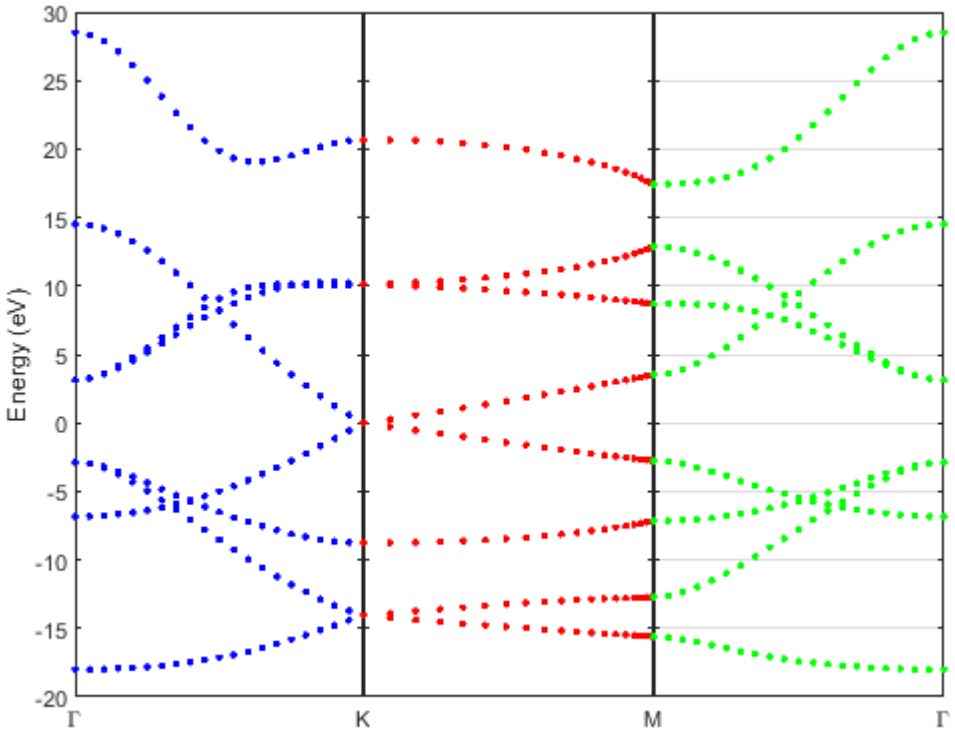

Figure 2.4: Band structure of monolayer graphene (up to 1NN interactions)

2.3 Bilayer Graphene

Bilayer graphene is essentially two monolayers stacked on top of each other and separated by a specified distance. We investigate two major configurations, AA and AB.

In AA stacking the monolayer lattices lie exactly above each other and have the same reflections in the horizontal plane, i.e a second monolayer is simply placed at a separation distance $c = 3.35\mathring{A}$, relative to the first. In AB stacking the second layer in addition to being shifted vertically, it's also shifted horizontally by a distance $a_1 = \frac{a}{\sqrt{3}}$. In these configurations the in-plane sp_2 hybrid orbital interactions are effectively untouched, and are just as shown in the monolayer band structure, so that we limit ourselves to the pi-orbital interactions in-plane and out-of-plane.

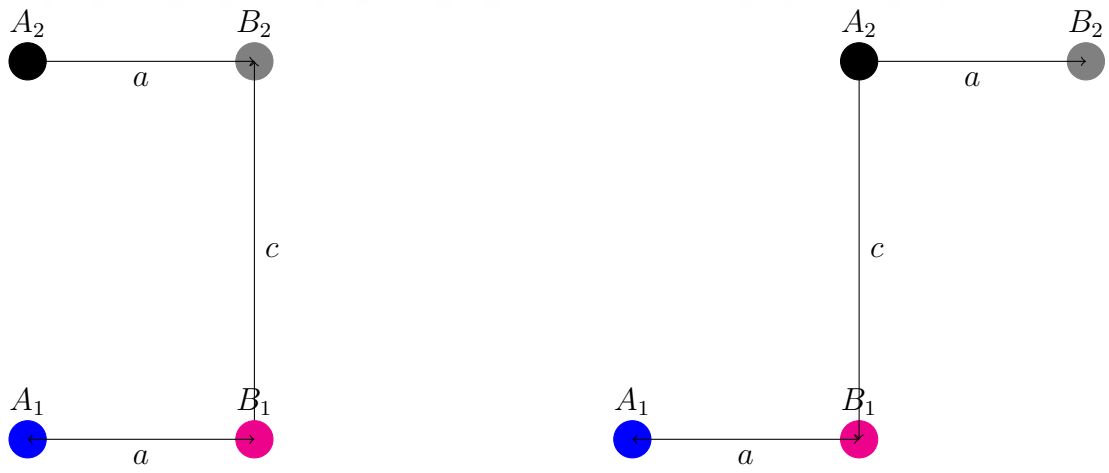

Figure 2.5: Side view of bilayer graphene:Arrangement of lattice generating four basis atoms shown.(Left) AA stacking and (right) AB stacking. Two basis atoms from each monolayer.

For 1NN interactions in-plane and out-of-plane, we construct the Hamiltonian

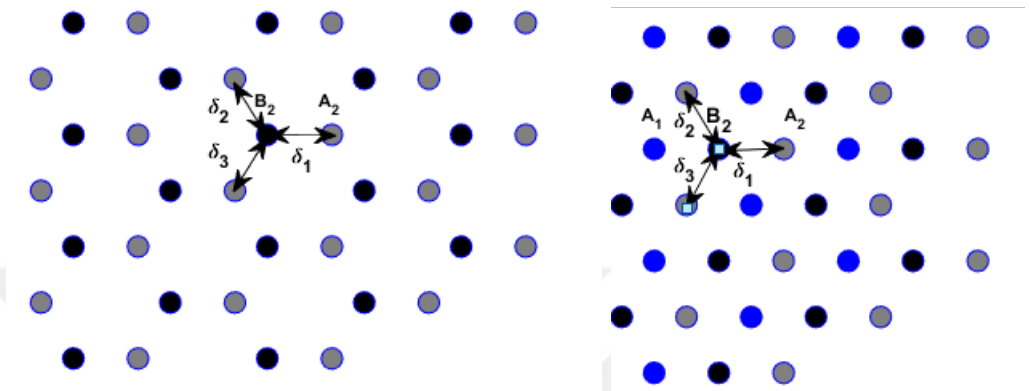

Figure 2.6: Top view:(Left) AA stacking. (right) AB stacking

and Overlap matrices,

$$H = \begin{bmatrix} H_{p_{z_{A_1}} p_{z_{A_1}}} & H_{p_{z_{A_1}} p_{z_{B_1}}} & H_{p_{z_{A_1}} p_{z_{A_2}}} & H_{p_{z_{A_1}} p_{z_{B_2}}} \\ H_{p_{z_{B_1}} p_{z_{A_1}}} & H_{p_{z_{B_1}} p_{z_{B_1}}} & H_{p_{z_{B_1}} p_{z_{A_2}}} & H_{p_{z_{B_1}} p_{z_{B_2}}} \\ H_{p_{z_{A_2}} p_{z_{A_1}}} & H_{p_{z_{A_2}} p_{z_{B_1}}} & H_{p_{z_{A_2}} p_{z_{A_2}}} & H_{p_{z_{A_2}} p_{z_{B_2}}} \\ H_{p_{z_{B_2}} p_{z_{A_1}}} & H_{p_{z_{B_2}} p_{z_{B_1}}} & H_{p_{z_{B_2}} p_{z_{A_2}}} & H_{p_{z_{B_2}} p_{z_{B_2}}} \end{bmatrix} \tag{2.47}$$

$$S = \begin{bmatrix} S_{p_{z_{A_1}} p_{z_{A_1}}} & S_{p_{z_{A_1}} p_{z_{B_1}}} & S_{p_{z_{A_1}} p_{z_{A_2}}} & S_{p_{z_{A_1}} p_{z_{B_2}}} \\ S_{p_{z_{B_1}} p_{z_{A_1}}} & S_{p_{z_{B_1}} p_{z_{B_1}}} & S_{p_{z_{B_1}} p_{z_{A_2}}} & S_{p_{z_{B_1}} p_{z_{B_2}}} \\ S_{p_{z_{A_2}} p_{z_{A_1}}} & S_{p_{z_{A_2}} p_{z_{B_1}}} & S_{p_{z_{A_2}} p_{z_{A_2}}} & S_{p_{z_{A_2}} p_{z_{B_2}}} \\ S_{p_{z_{B_2}} p_{z_{A_1}}} & S_{p_{z_{B_2}} p_{z_{B_1}}} & S_{p_{z_{B_2}} p_{z_{A_2}}} & S_{p_{z_{B_2}} p_{z_{B_2}}} \end{bmatrix} \tag{2.48}$$

Where for AA stacking,

$$H_{p_{z_{A_1}} p_{z_{B_1}}} = H_{48} \tag{2.49}$$

$$H_{p_{z_{A_2}} p_{z_{B_2}}} = H_{48}^* \tag{2.50}$$

$$H_{p_{z_{A_1}} p_{z_{A_2}}} = V_1 e^{-ik_z c} \left(e^{-i\frac{k_x a}{\sqrt{3}}} + 2e^{i\frac{k_x a}{2\sqrt{3}}} \cos\left(\frac{k_y a}{2}\right) \right) \tag{2.51}$$

$$H_{p_{z_{A_1}} p_{z_{B_2}}} = H_{p_{z_{B_1}} p_{z_{A_2}}} = V_2 e^{-ik_z c} \tag{2.52}$$

$$H_{p_{z_{B_1}} p_{z_{B_2}}} = V_1 e^{-ik_z c} \left(e^{i\frac{k_x a}{\sqrt{3}}} + 2e^{-i\frac{k_x a}{2\sqrt{3}}} \cos\left(\frac{k_y a}{2}\right) \right) \tag{2.53}$$

$$\tag{2.54}$$

For AB stacking

$$H_{p_{z_{A_1}} p_{z_{B_1}}} = H_{48} \tag{2.55}$$

$$H_{p_{z_{A_2}} p_{z_{B_2}}} = H_{48}^* \tag{2.56}$$

$$H_{p_{z_{A_1}} p_{z_{A_2}}} = V_1 e^{-ik_z c} \left(e^{i\frac{k_x a}{\sqrt{3}}} + 2e^{-i\frac{k_x a}{2\sqrt{3}}} \cos\left(\frac{k_y a}{2}\right)\right) \tag{2.57}$$

$$H_{p_{z_{A_1}} p_{z_{B_2}}} = V_1 e^{-ik_z c} \left(e^{-i\frac{k_x a}{\sqrt{3}}} + 2e^{i\frac{k_x a}{2\sqrt{3}}} \cos\left(\frac{k_y a}{2}\right)\right) \tag{2.58}$$

$$H_{p_{z_{B_1}} p_{z_{B_2}}} = V_2 e^{-ik_z c} \tag{2.59}$$

$$\tag{2.60}$$

and for both, as similarly applied

$$H_{p_{z_{A_2}} p_{z_{A_1}}} = H^*_{p_{z_{A_1}} p_{z_{A_2}}}, H_{p_{z_{B_2}} p_{z_{A_1}}} = H^*_{p_{z_{A_1}} p_{z_{B_2}}}, H_{p_{z_{A_2}} p_{z_{B_1}}} = H_{p_{z_{B_1}} p_{z_{A_2}}}*,$$
$$H_{p_{z_{B_2}} p_{z_{B_1}}} = H_{p_{z_{B_1}} p_{z_{B_2}}}* \tag{2.61}$$

$V_1 = 0.39$ and $V_2 = 0.315$ [4] and apart from the non-zero elements which were defined for monolayer graphene the other elements of the overlap matrix are zero. In bilayer graphene, the band structure along direction $\Gamma - K - M$ localized on the edge of a triangle as shown, where

$$\Gamma = \left(0, 0, \frac{\pi}{c}\right), K = \left(\frac{2\pi}{\sqrt{3}a}, -\frac{2\pi}{3a}, \frac{\pi}{c}\right), M = \left(\frac{2\pi}{\sqrt{3}a}, 0, \frac{\pi}{c}\right) \tag{2.62}$$

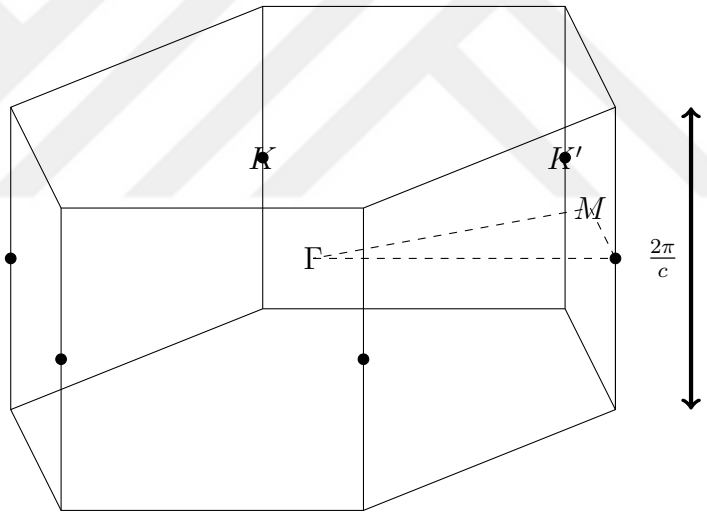

Figure 2.7: First Brilloiun zone graphite

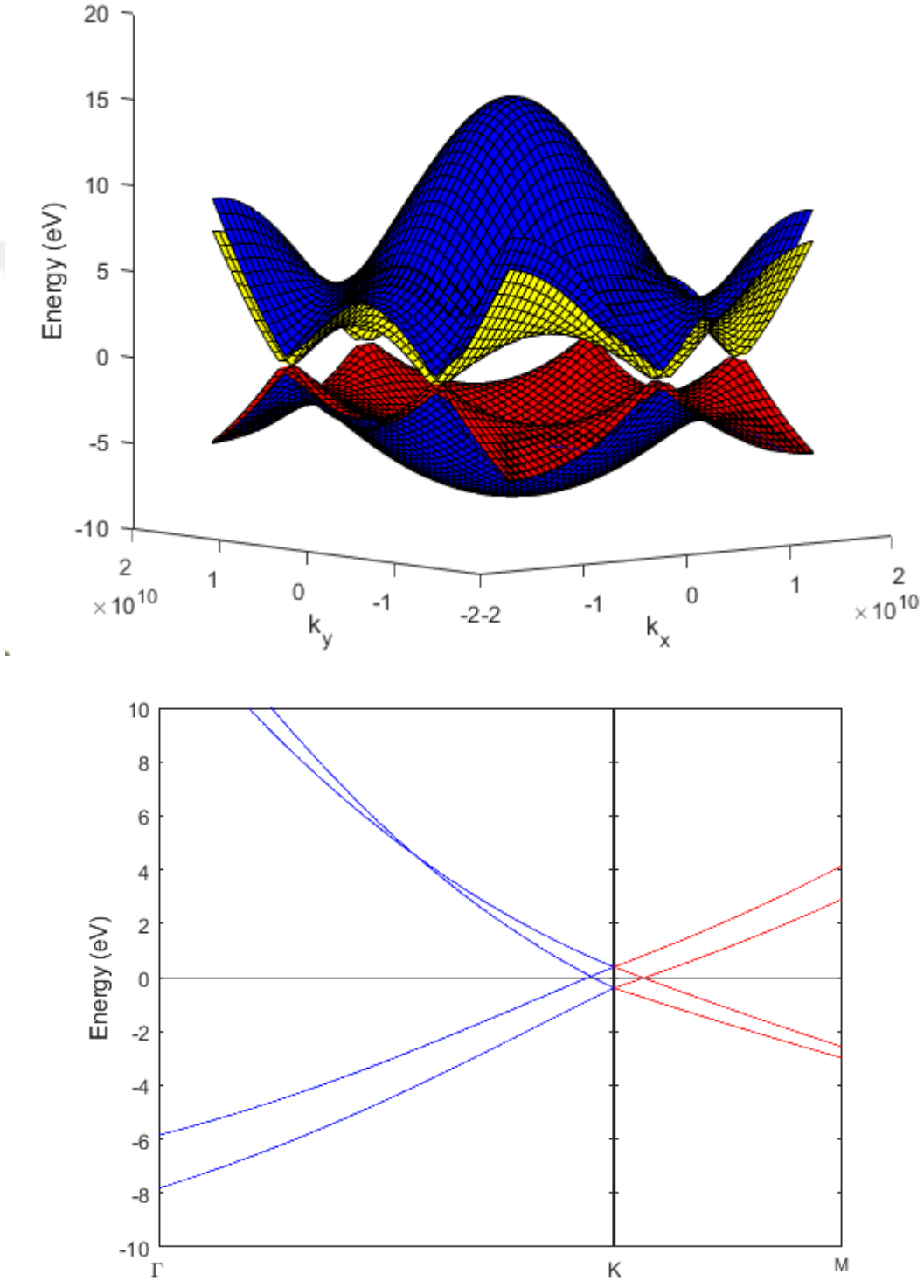

Figure 2.8: Electronic band structure AA stacking: (top) 3D band structure. (bottom) 2D along $\Gamma - K - M$ directions

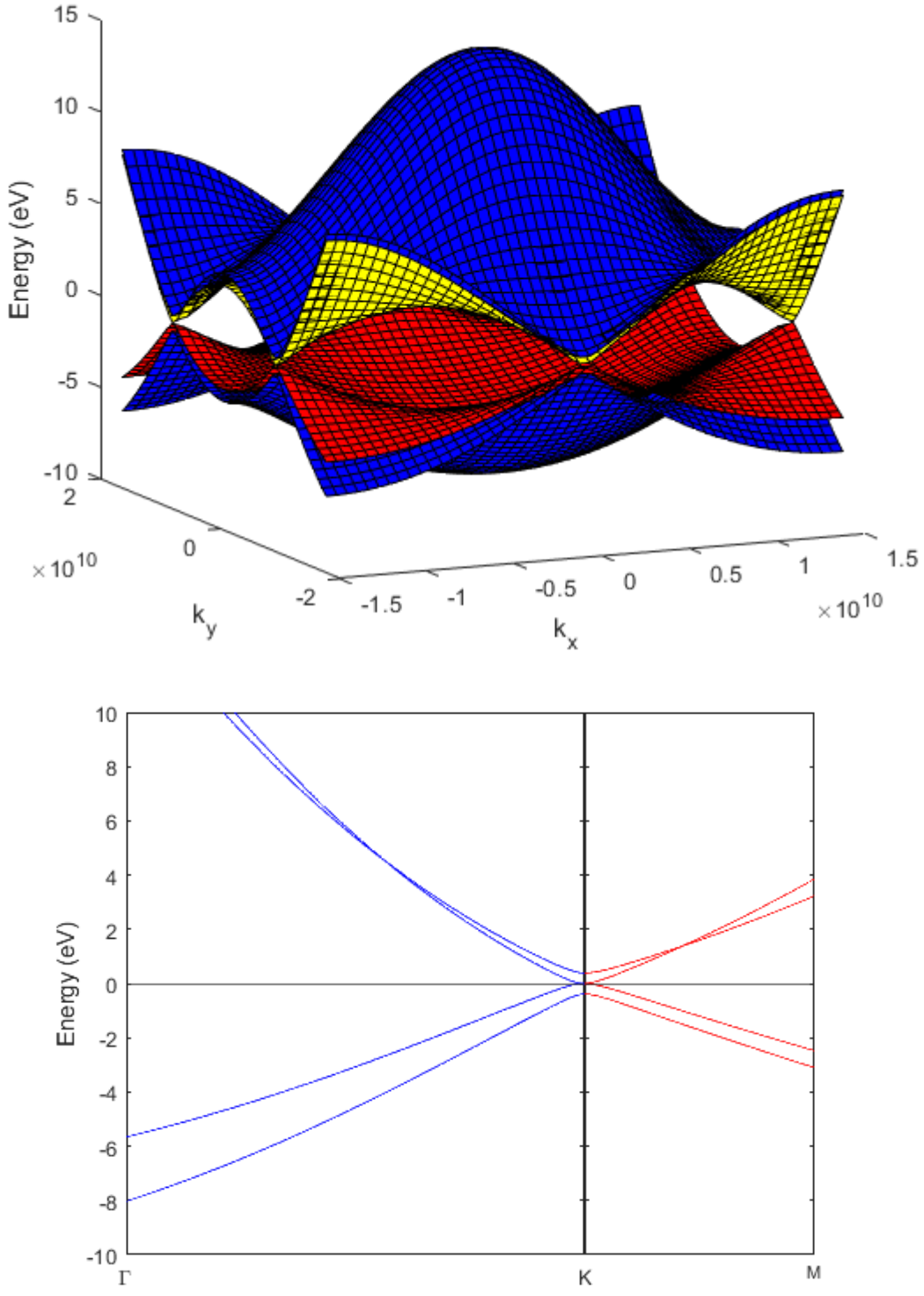

Figure 2.9: Electronic band structure of AB stacking: (top) 3D band structure. (bottom) 2D along $\Gamma - K - M$ directions

Chapter 3

Dynamics of Sliding and Loading Bilayer Graphene

One of the major problems of the tight-binding approach to electronic band structure calculations is the determination of suitable tight-binding parameters for various intra and inter atomic orbital interactions. Generally, researchers find suitably fitted tight binding parameters for the high symmetry points, from the band structure results of other semi-empirical, first-principle and experimental methods. At least by fitting, the resulting band structure behaves well in the vicinity of the high symmetry points. It's quite difficult to find models that produce suitable tight binding parameters over a continuous range of interatomic interacting distances.

For sliding bilayer graphene- A monolayer, relative to the other, is shifted in a direction parallel to the horizontal plane, or loading bilayer graphene- A monolayer, relative to the other is shifted in a direction normal to horizontal plane, calculating the electronic band structure gets difficult, since we have to compute both $H_{pp\sigma}$ and $H_{pp\pi}$ for any two interacting atoms in a system for which the electronic band structure is to be calculated, particularly because the relative angle changes for each pair of interacting orbitals change for both sliding and drifting bilayer graphene.

In our modelling of the p_z orbital interactions, motivated by the exponential dependence of hydrogen-like orbital wavefunctions, we resolve to find suitable exponential functions similar to that reported by [20, 21] for both $H_{pp\sigma}$ and $H_{pp\pi}$ in the form $H = e^{\frac{b(d-\mu)}{u}}$. We first try to model the $H_{pp\pi}$ parameters, in which case for interaction distances $d \geq a$ they can be at least one order of magnitude smaller than corresponding $H_{pp\sigma}$ parameters. In seeking a model for $H_{pp\pi}$ parameters we make use of the parameters $\gamma_0 = -2.78eV, \gamma_1 = -0.12eV, \gamma_2 = -0.068eV$ for 1NN, 2NN and 3NN in-plane π interactions respectively [22]. Similarly with the help of eq. 2.19, we use the values $\gamma_0^{'} = 5.10eV$[19], $\gamma_1^{'} = 0.39eV \gamma_3^{'} = 0.371eV, \gamma_5^{'} = 0.038eV$ [4] for interaction distances $1.42\mathring{A}$, $3.35\mathring{A}$, $3.639\mathring{A}$, $6.70\mathring{A}$ respectively. We obtain the exponential functions,

$$H_{pp\sigma} = U_{pp\sigma} e^{\frac{b_{pp\sigma}(d-\mu_{pp\sigma})}{\sigma_{pp\sigma}}} \tag{3.1}$$

$$H_{pp\pi} = U_{pp\pi} e^{\frac{b_{pp\pi}(d-\mu_{pp\pi})}{\sigma_{pp\pi}}}, \tag{3.2}$$

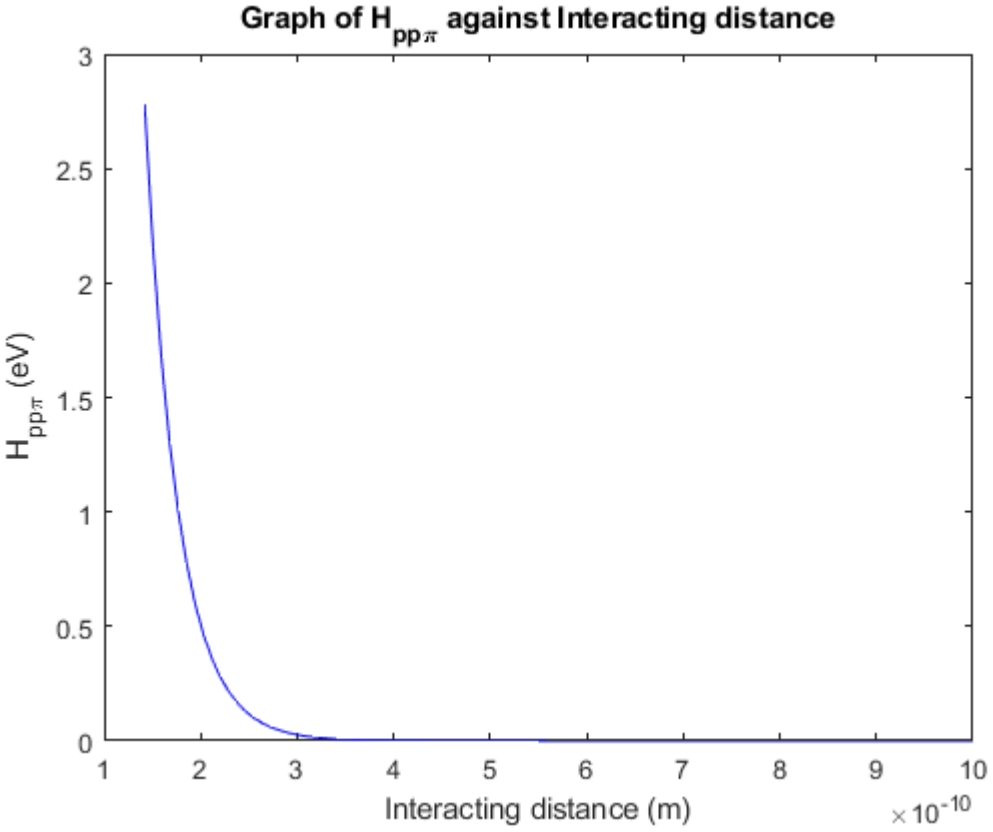

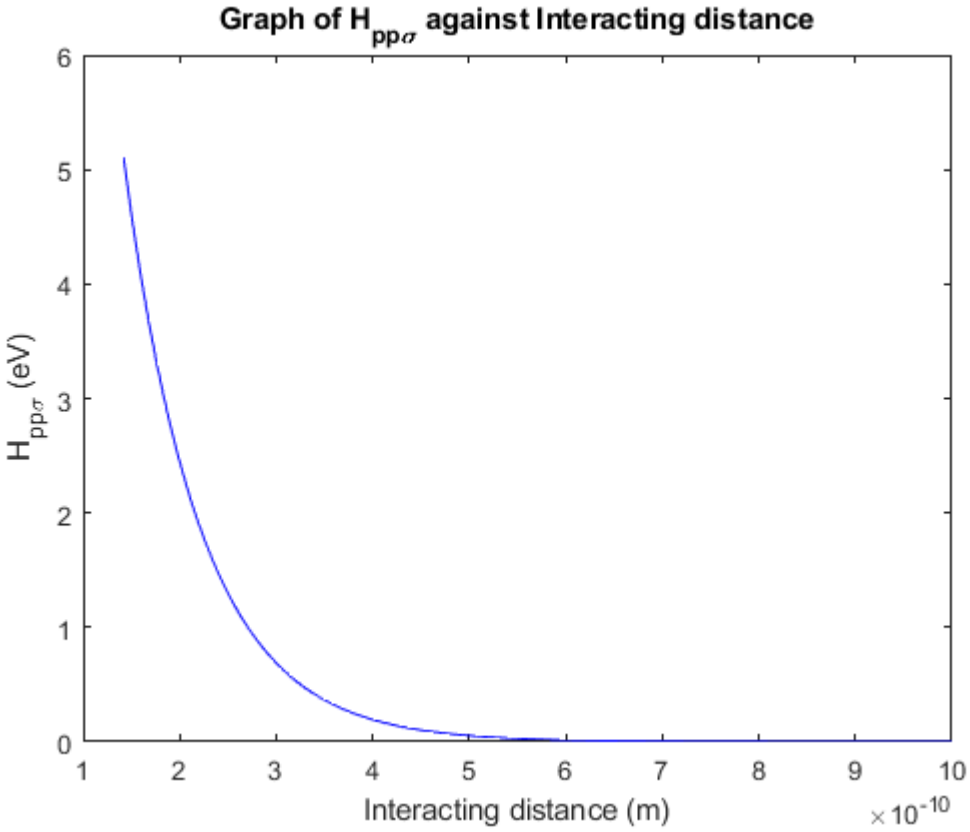

Figure 3.1: (top) Graphs $H_{pp\sigma}$ against interaction distance. (bottom) Graph of $H_{pp\pi}$ against interacting distance

where $b_{pp\sigma} = -2.766$, $b_{pp\pi} = -2.159$, $b_{pp\sigma} = -2.766$, $\mu_{pp\sigma} = 3.777 \cdot 10^{-10}m$, $\mu_{pp\pi} = 2.24{\cdot}10^{-10}m$, $\sigma_{pp\sigma} = 2.183{\cdot}10^{-10}m$, $\sigma_{pp\pi} = 7.352{\cdot}10^{-11}m$, $U_{pp\sigma} = 0.2574eV$, $U_{pp\pi} = 0.2502eV$

When we specify the maximum number of nearest neighbour interactions considered in our band structure analysis of sliding or loading bilayer graphene, at least two things are possible. The interacting distance between atoms may change and the number of atoms at an nth nearest neighbour interacting distance may change. We observe that the latter case while being at play in sliding bilayer graphene, it isn't in loading bilayer graphene. We do our tight-binding calculations for 2NN and 4NN interactions in-plane and out-of-plane, however only

the graphs for 4NN interactions are provided. Note that for out-of-plane interactions, nearest neighbour atoms are all at the same interacting distance and of the same sub-lattice type. One of the reasons for doing tight-binding calculations for 4NN interactions is to ensure that we include as many interactions as possible so that the changes in the number of atoms per group of nearest neighbour atoms does not significantly affect the changes in band structure. In which case such a problem cannot be avoided for 2NN interactions in-plane and out-of-plane for example. However doing tight binding calculations for both of them allows us to be able determine if changing the number of nearest neighbour atoms affects the accuracy of our band structure graphs as we try to compare them to results obtainable from literature.

3.1 Sliding Bilayer Graphene

Given the tight-binding parameter functions, we seek to investigate the change in the band structure of a sliding bilayer in three different directions:x-direction, y-direction and diagonal direction. We denote sliding in the x-directions and y-direction by x-shifts and y-shifts respectively. For the directions shown in Fig. 3.2, and assuming we commence sliding from AA stacking, we observe x-shifts of the upper monolayer in intervals of $\frac{a}{10\sqrt{3}}$ over the range $\left[0, \frac{a}{\sqrt{3}}\right]$ and y-shifts in intervals of $\frac{a}{10}$ over the range $[0, a]$, where $a = 2.46\mathring{A}$, graphene lattice parameter. One observation is that for the three different shift directions, band splittings are generated in the bilayer electronic band structure, even increasing over a range of shifts in the different directions. It's important to note also that the band splitting generated in the first BZ direction, $\Gamma - K$ is different from the BZ edge direction $K - M$.

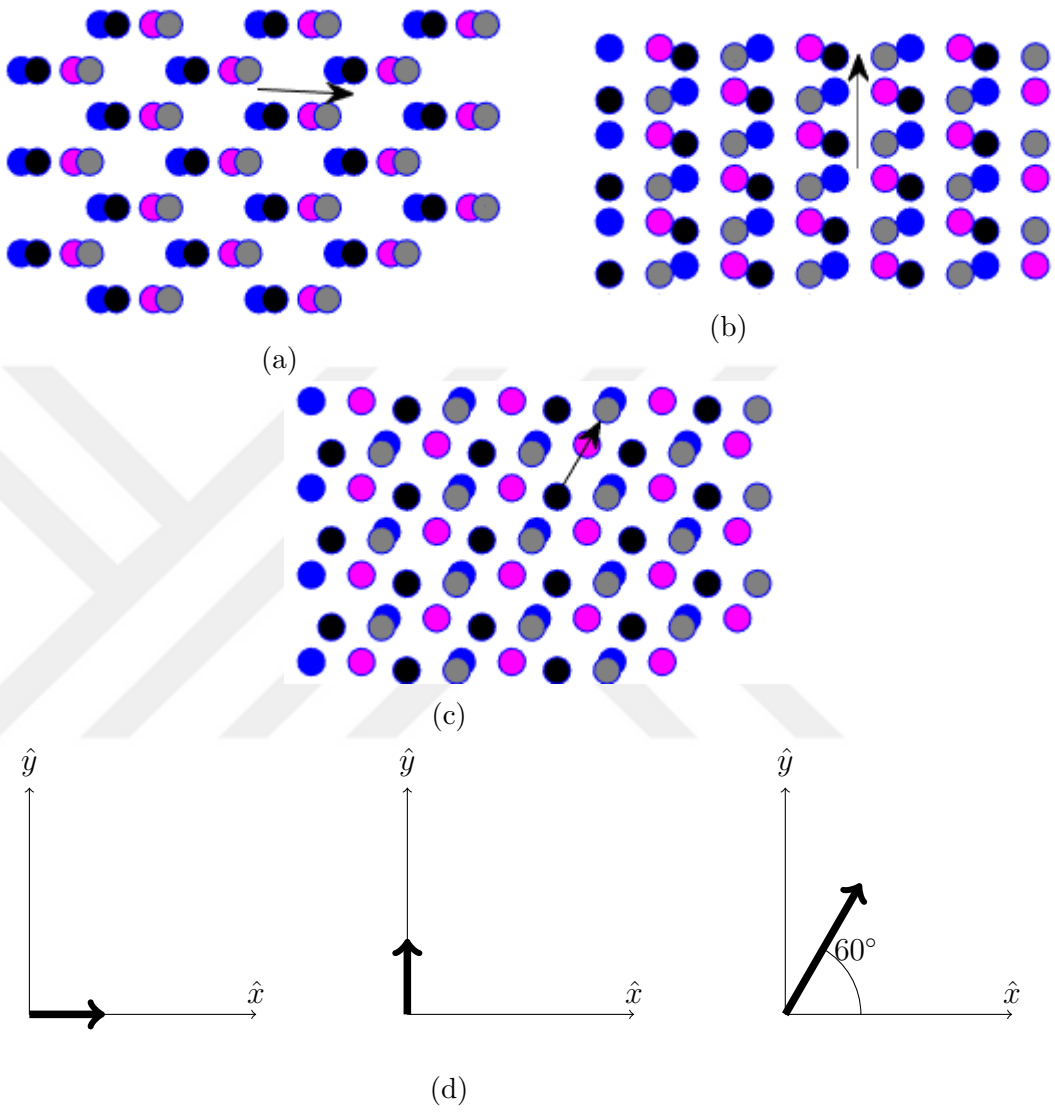

Figure 3.2: Three different upper monolayer sliding directions:(a) Sliding along x-direction. (b) Sliding along y-direction. (c) Sliding along diagonal direction. (d) The respective direction are shown from (left) to (right)

Our calculations for shifts in the x-direction, shown in Table. 3.2 indicate two groups of x-shifts that show increasing band gaps for both the $\Gamma - K$ and $K - M$ directions. The band gap increases on the ranges $\left[0, \frac{3a}{10\sqrt{3}}\right]$, and $\left[\frac{4a}{10\sqrt{3}}, \frac{7a}{10\sqrt{3}}\right]$. The results from sliding bilayer and the 3D graphs in Figs. (2.8) and (2.9) indicate that what we see for AA stacking is the lower conduction and valence band sheets caving inwards in the vicinity of K, with circles of energy points surrounding the K point, so that what you have in that neighbourhood is a cone sitting on another

with zero band splitting. Apart from the fact that no band splittings are seen in the direction $K - M$, no notable patterns in band splittings changes are seen for y-shifts. For shifts in the diagonal direction, a pattern of increasing band gaps appear between $\Gamma - K$ and $K - M$ directions, for shifts $(0, 0)$ and $\left(\frac{3a}{10\sqrt{3}}, \frac{3a}{10}\right)$. The band gaps indicated with the asterisk are the seemingly indirect band gaps, although we purport here we may be dealing with band crossings.

Band splitting (eV)		
Shift	$\Gamma - K$	$K - M$
0	0.000	0.000
$\frac{a}{10\sqrt{3}}$	0.025	0.047
$\frac{2a}{10\sqrt{3}}$	0.044	0.091
$\frac{3a}{10\sqrt{3}}$	0.059	0.131
$\frac{4a}{10\sqrt{3}}$	0.041	0.091
$\frac{5a}{10\sqrt{3}}$	0.050	0.109
$\frac{6a}{10\sqrt{3}}$	0.066	0.113
$\frac{7a}{10\sqrt{3}}$	0.068	0.131
$\frac{8a}{10\sqrt{3}}$	0.059	0.089
$\frac{9a}{10\sqrt{3}}$	0.038	0.045
$\frac{a}{\sqrt{3}}$	0.000	0.000

Table 3.1: Table of band splitting values for top layer shifts with respect to the bottom layer along the x-direction

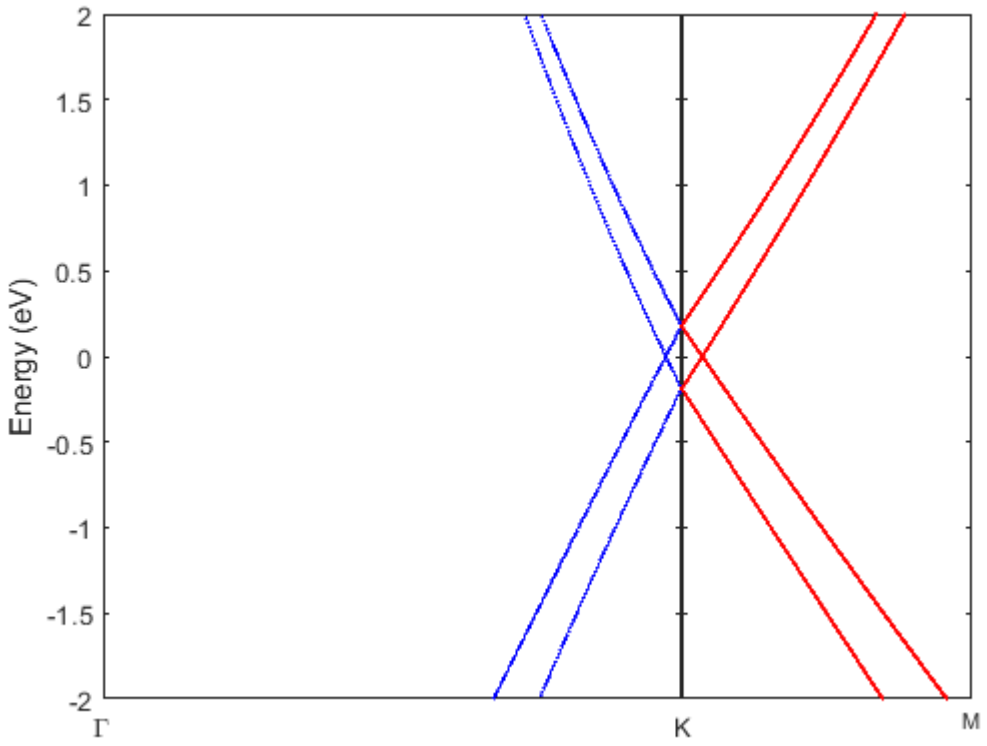

(a) $\Delta x = 0$

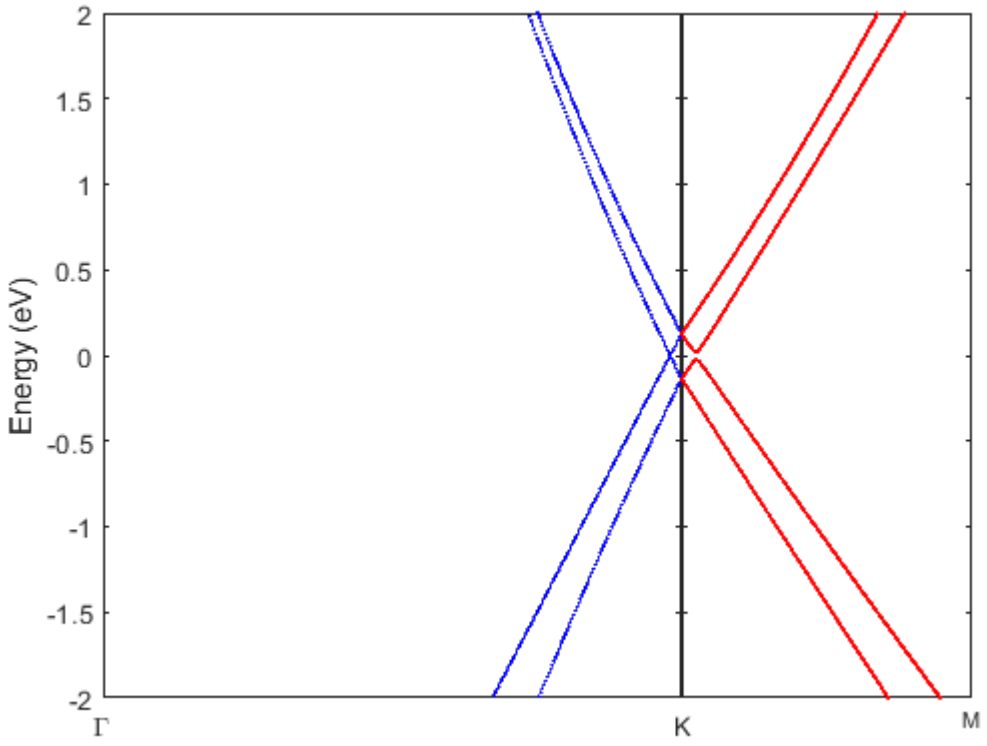

(b) $\Delta x = \frac{a}{10\sqrt{3}}$

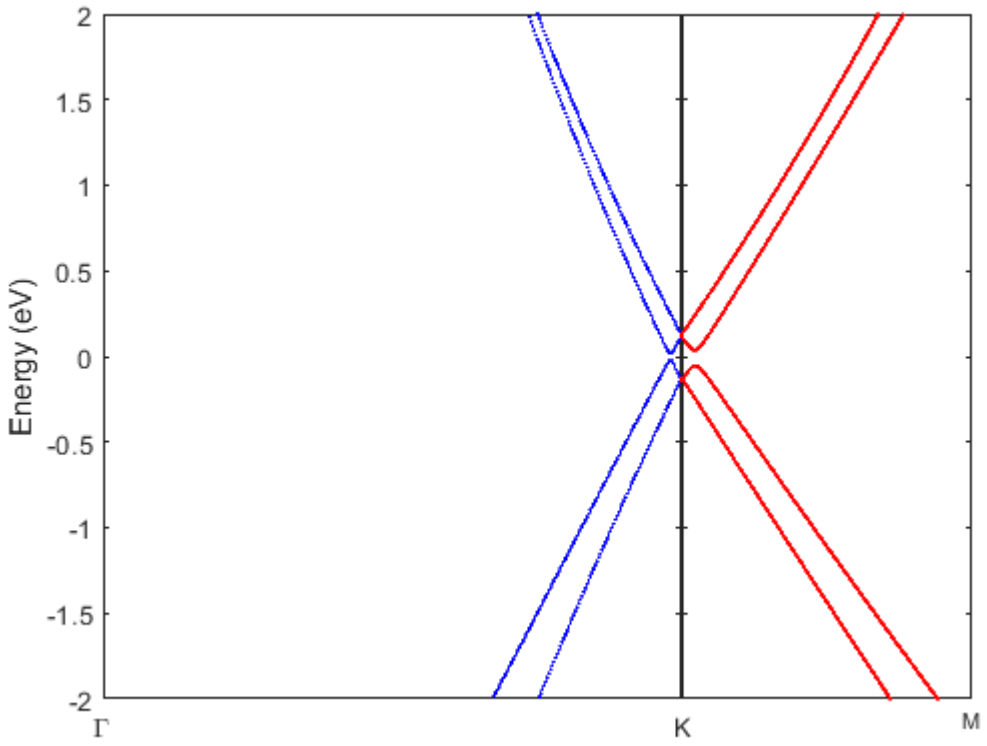

(c) $\Delta x = \frac{2a}{10\sqrt{3}}$

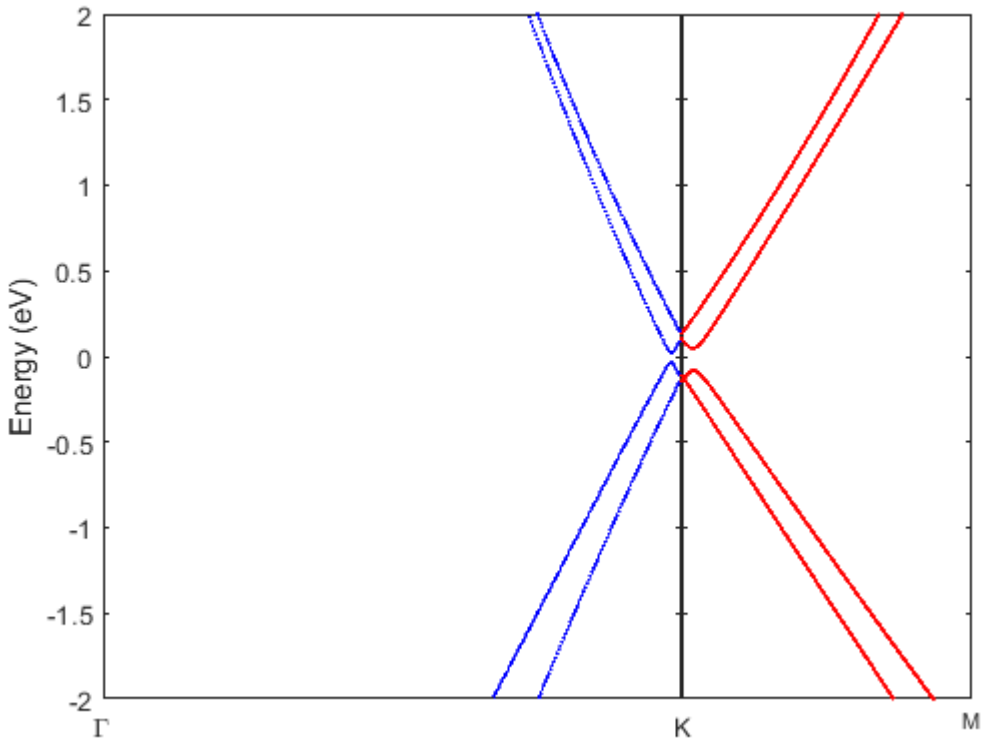

(d) $\Delta x = \frac{3a}{10\sqrt{3}}$

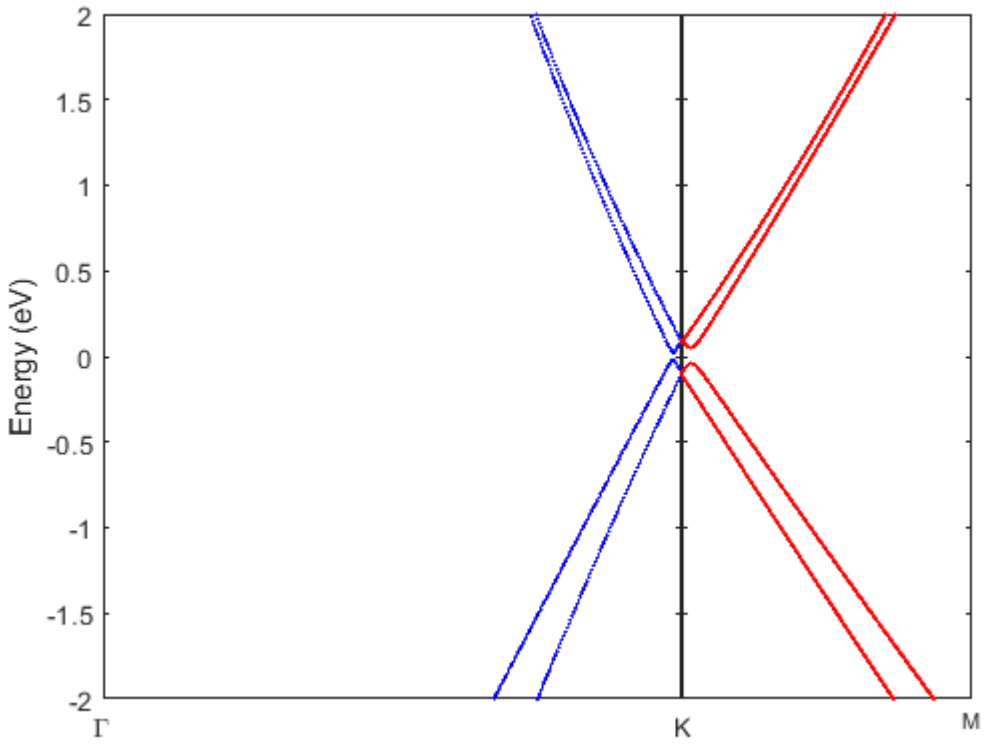

(e) $\Delta x = \frac{4a}{10\sqrt{3}}$

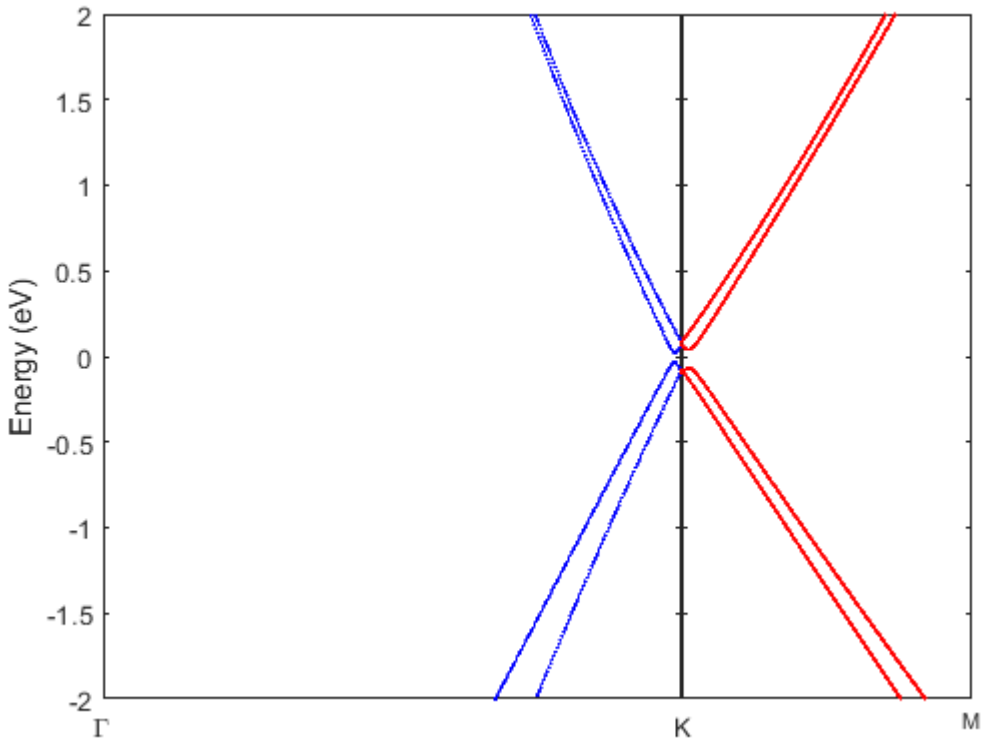

(f) $\Delta x = \frac{5a}{10\sqrt{3}}$

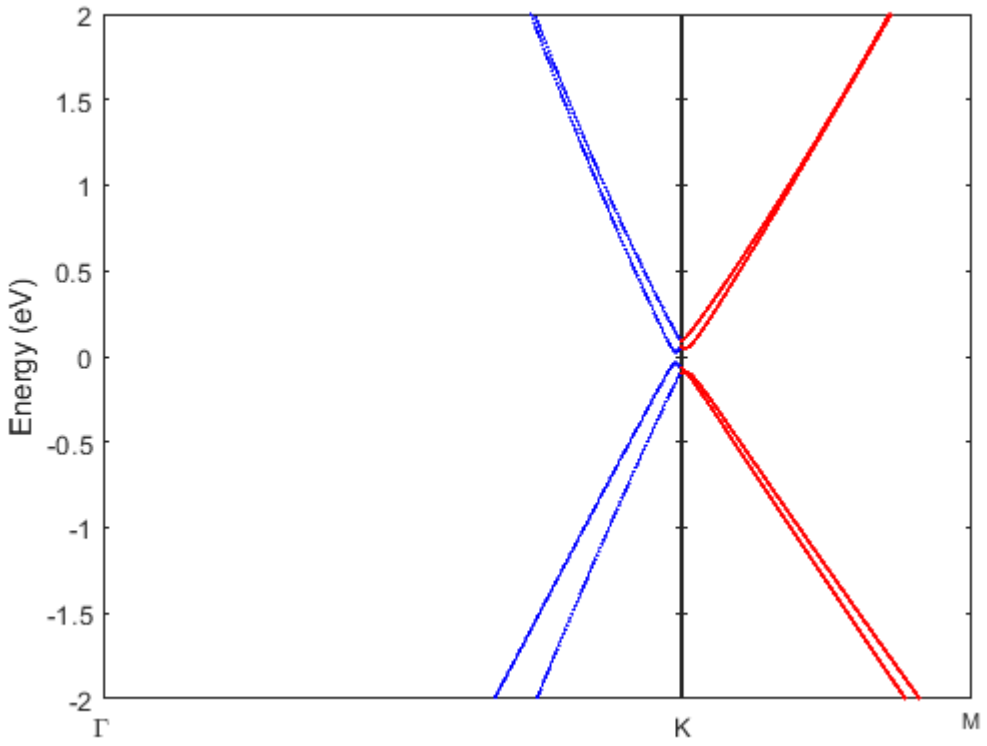

(g) $\Delta x = \frac{6a}{10\sqrt{3}}$

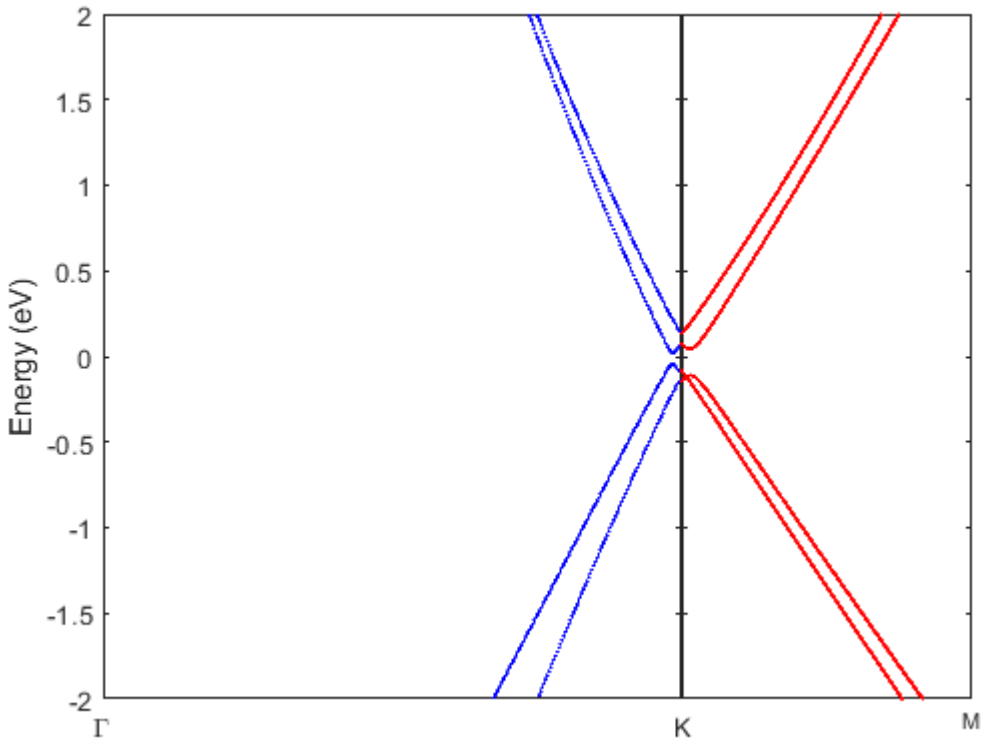

(h) $\Delta x = \frac{7a}{10\sqrt{3}}$

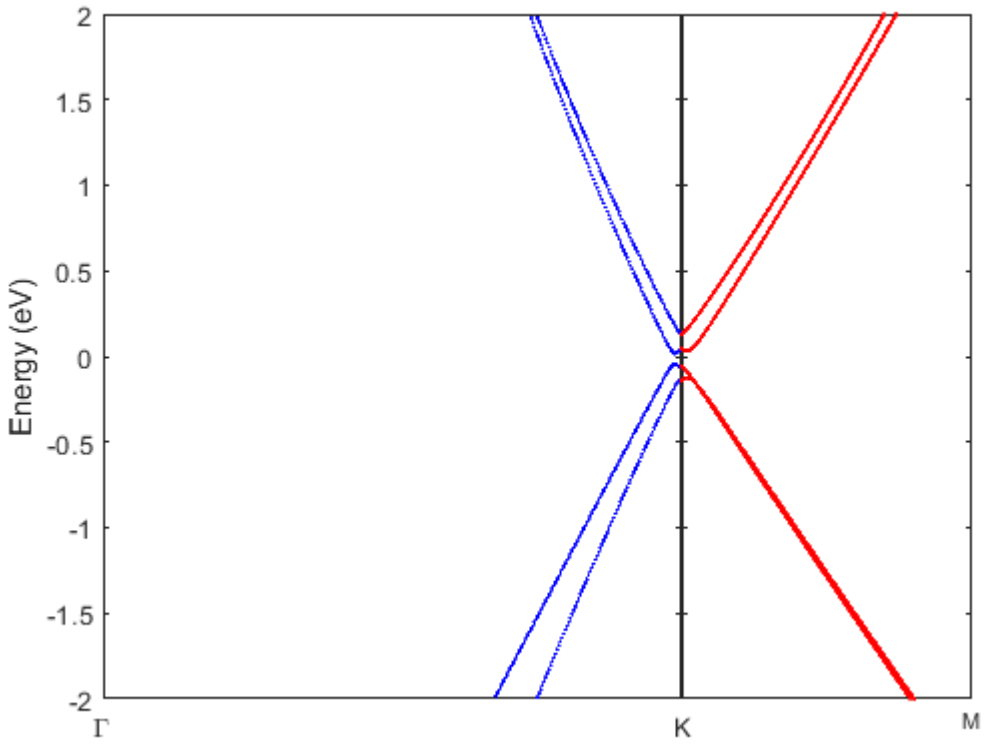

(i) $\Delta x = \frac{8a}{10\sqrt{3}}$

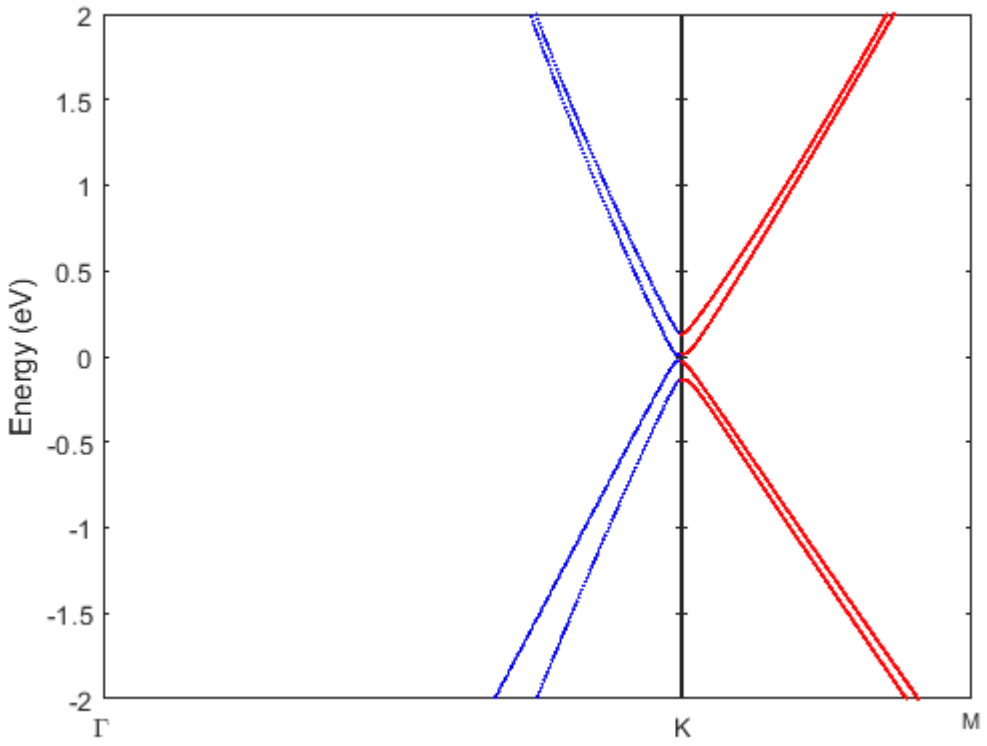

(j) $\Delta x = \frac{9a}{10\sqrt{3}}$

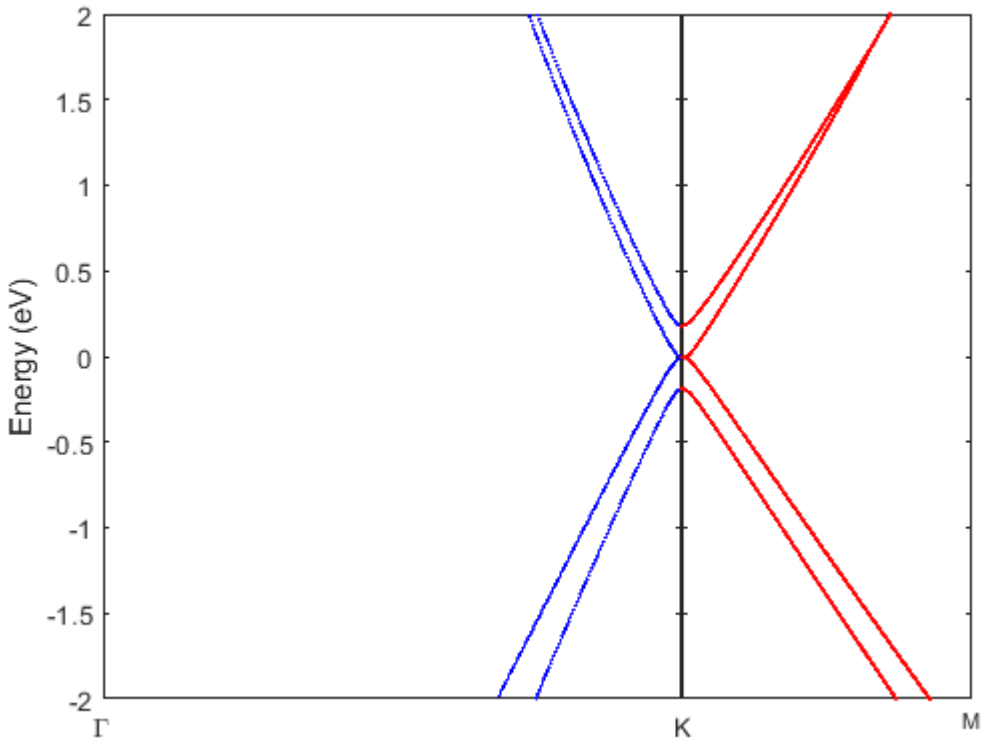

(k) $\Delta x = \frac{a}{\sqrt{3}}$

Figure 3.3: Shift in the x direction in intervals of $\frac{a}{10\sqrt{3}}$ from 0 to $\frac{a}{\sqrt{3}}$, corresponding to AA and AB configurations respectively

Band splitting (eV)		
Shift	$\Gamma - K$	$K - M$
0	0.000	0.000
$\frac{a}{10\sqrt{3}}$	0.025	0.047
$\frac{2a}{10\sqrt{3}}$	0.044	0.091
$\frac{3a}{10\sqrt{3}}$	0.059	0.131
$\frac{4a}{10\sqrt{3}}$	0.041	0.091
$\frac{5a}{10\sqrt{3}}$	0.050	0.109
$\frac{6a}{10\sqrt{3}}$	0.066	0.113
$\frac{7a}{10\sqrt{3}}$	0.068	0.131
$\frac{8a}{10\sqrt{3}}$	0.059	0.089
$\frac{9a}{10\sqrt{3}}$	0.038	0.045
$\frac{a}{\sqrt{3}}$	0.000	0.000

Table 3.2: Table of band splitting values for top layer shifts with respect to the bottom layer along the x-direction

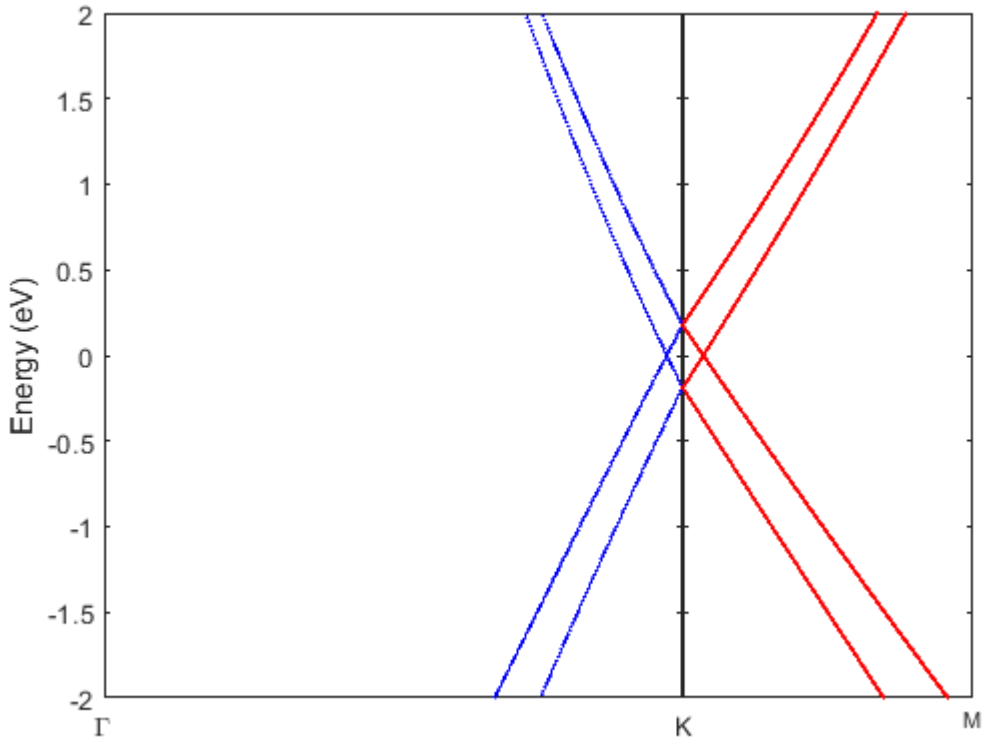

(a) $\Delta y = 0$

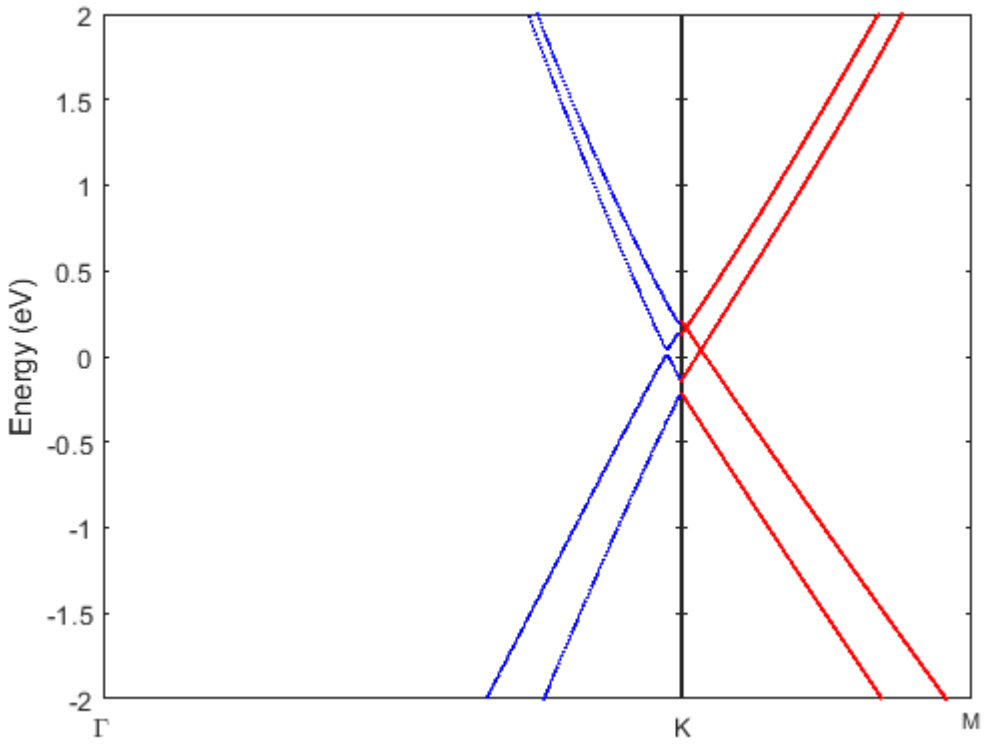

(b) $\Delta y = \frac{a}{10}$

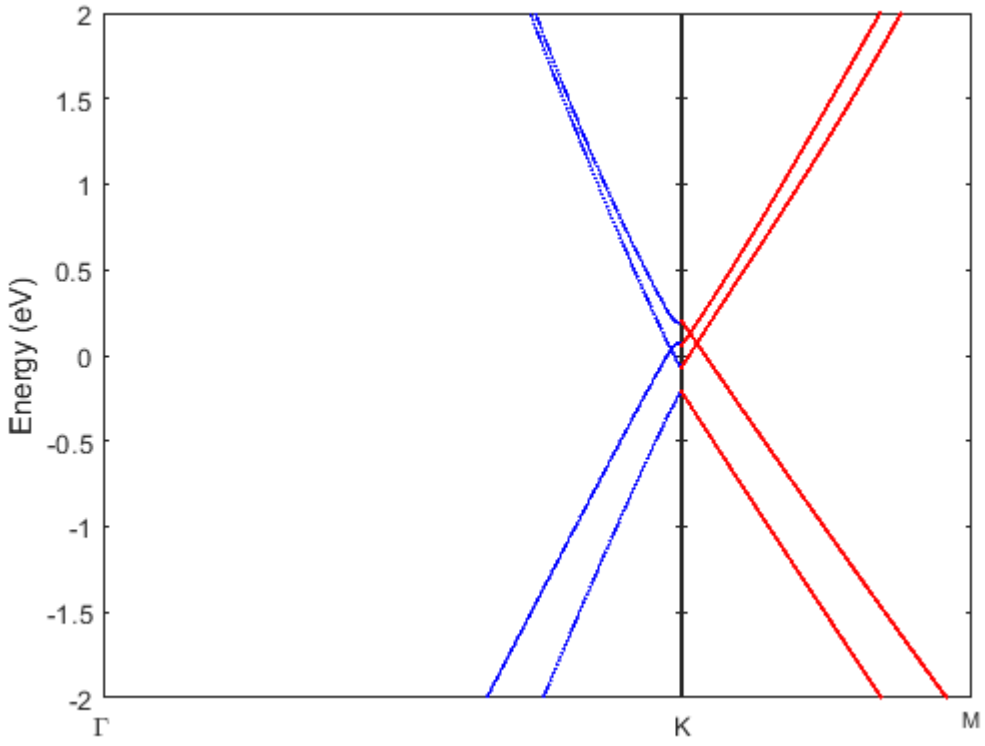

(c) $\Delta y = \frac{2a}{10}$

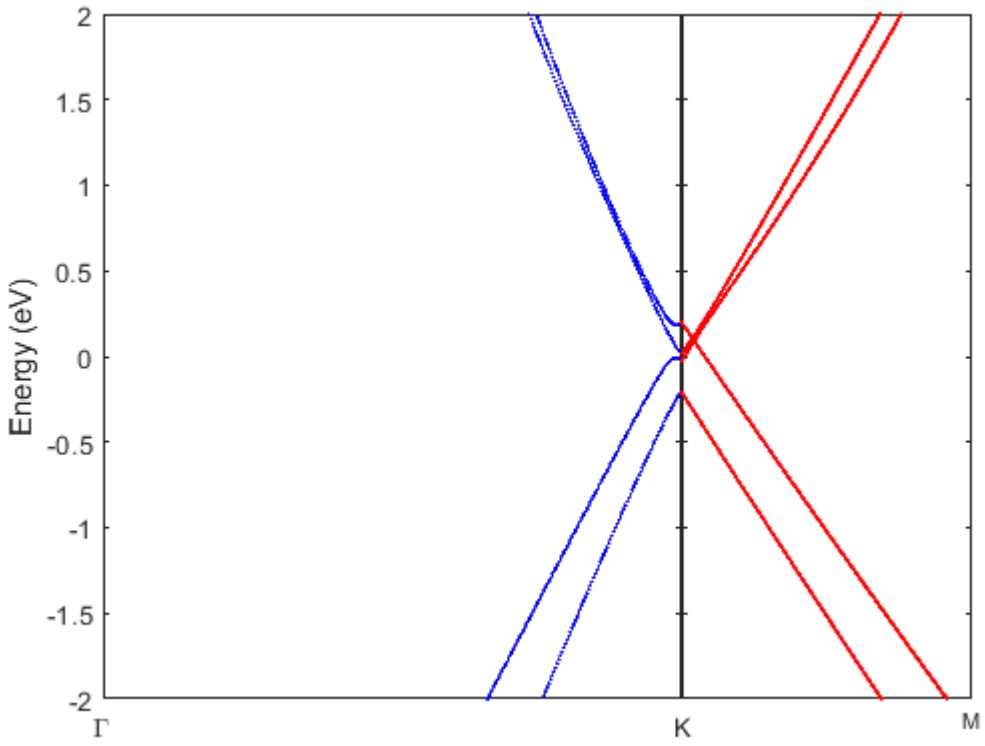

(d) $\Delta y = \frac{3a}{10}$

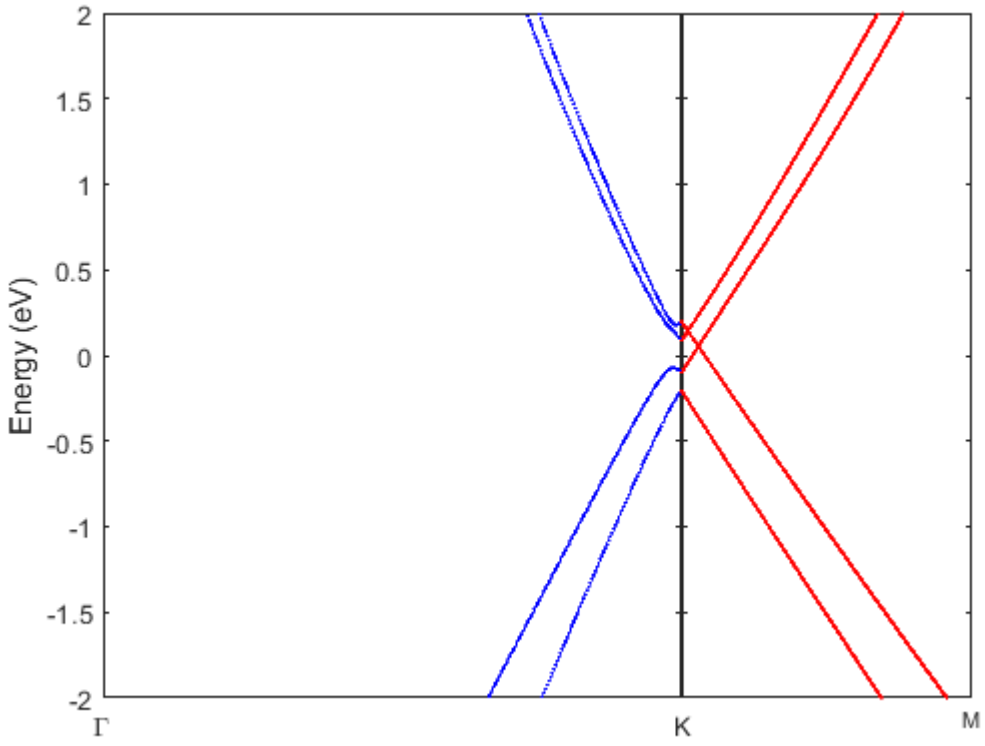

(e) $\Delta y = \frac{4a}{10}$

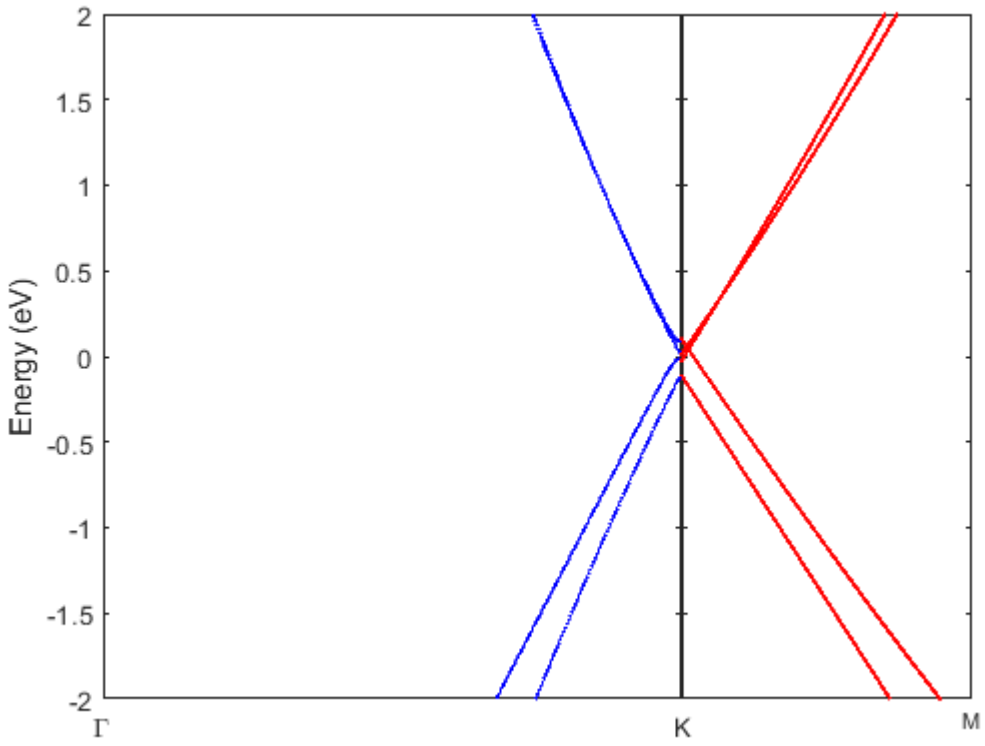

(f) $\Delta y = \frac{5a}{10}$

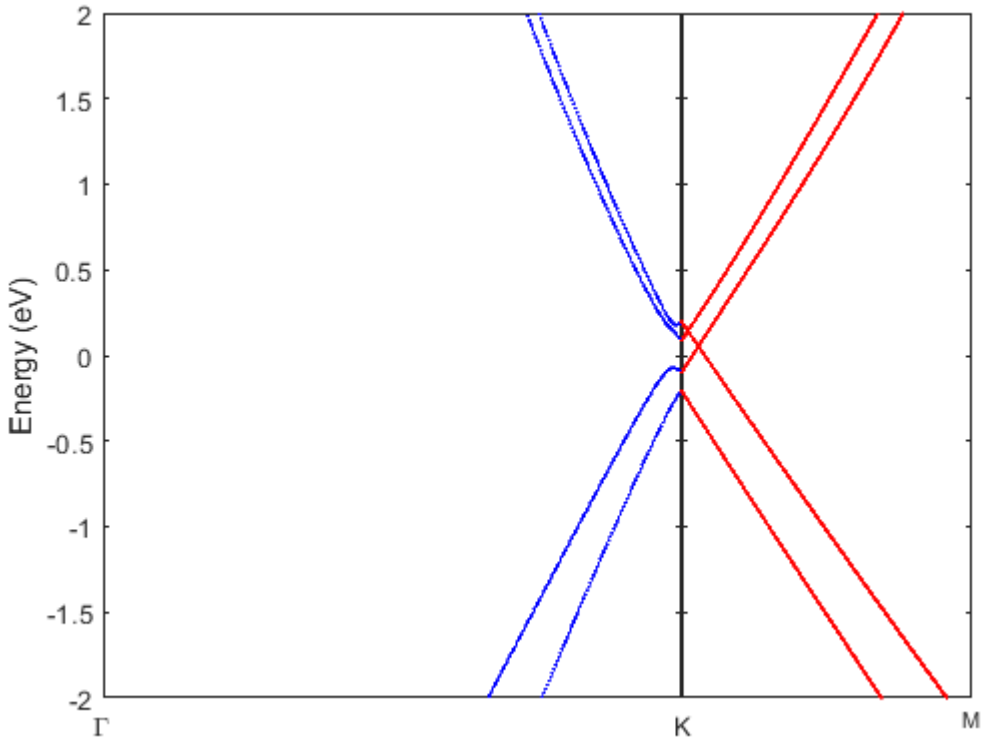

(g) $\Delta y = \frac{6a}{10}$

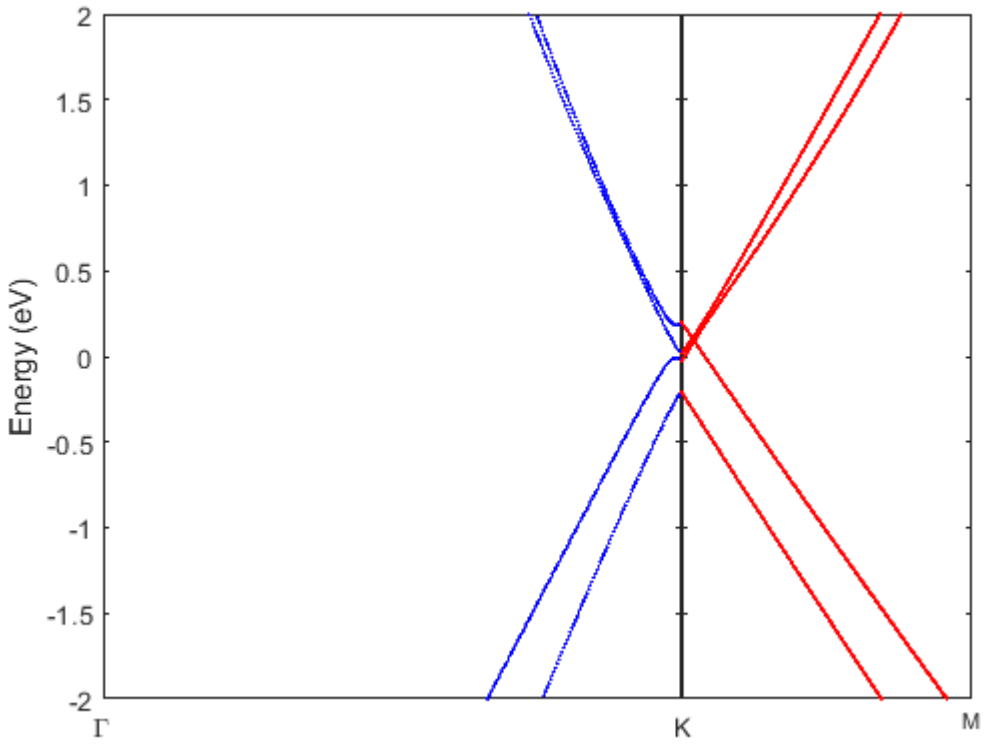

(h) $\Delta y = \frac{7a}{10}$

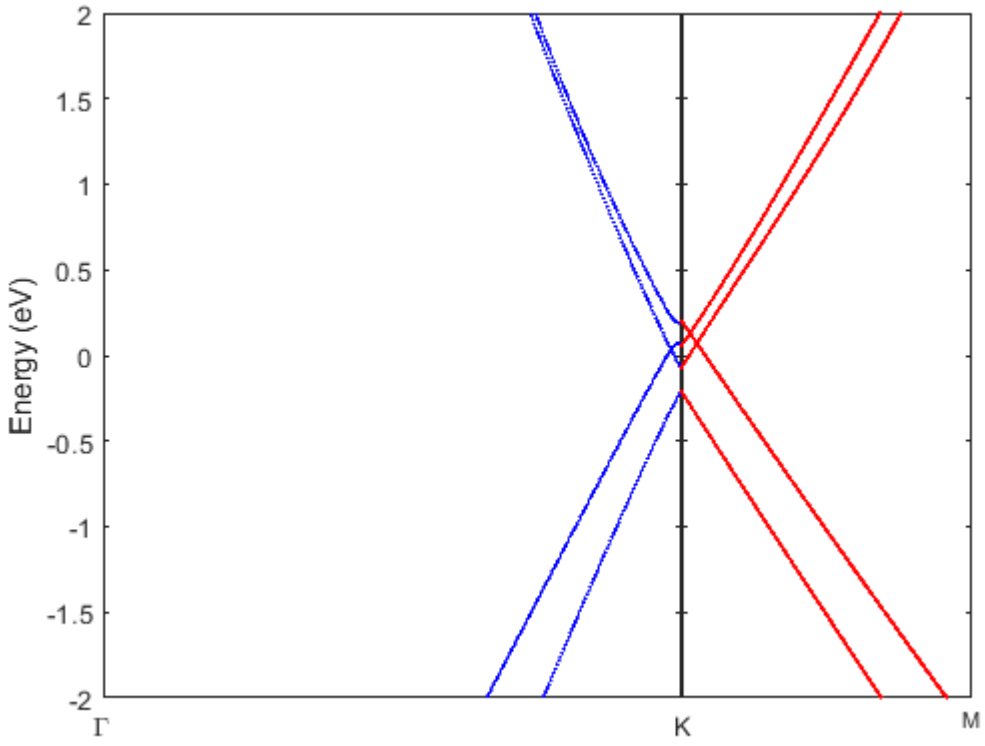

(i) $\Delta y = \frac{8a}{10}$

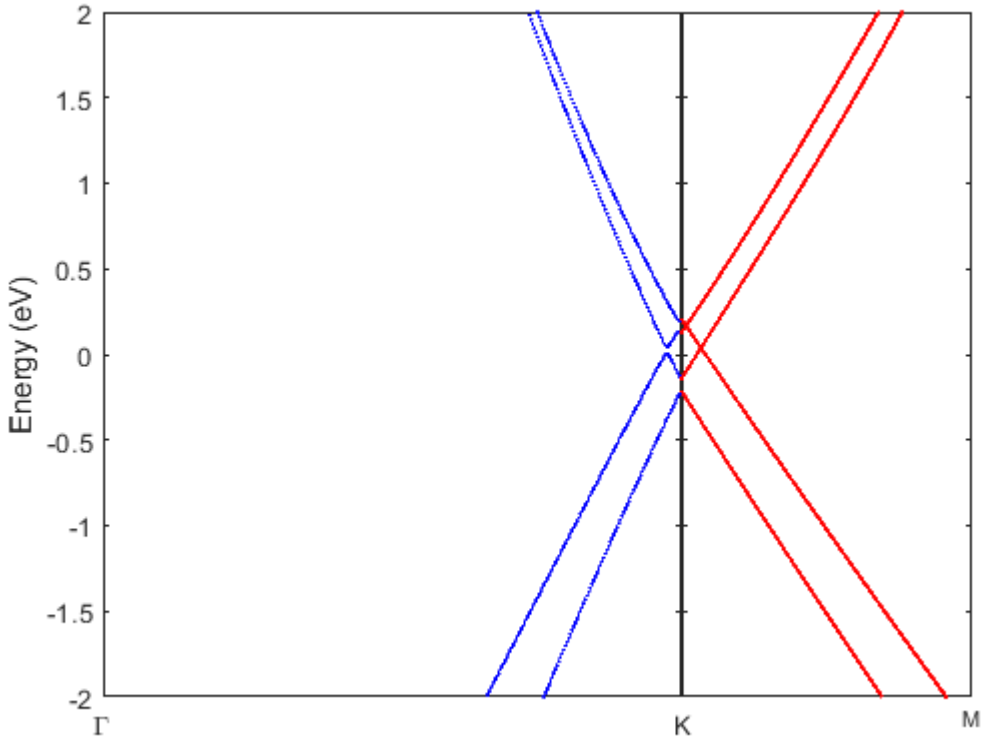

(a) $\Delta y = \frac{9a}{10}$

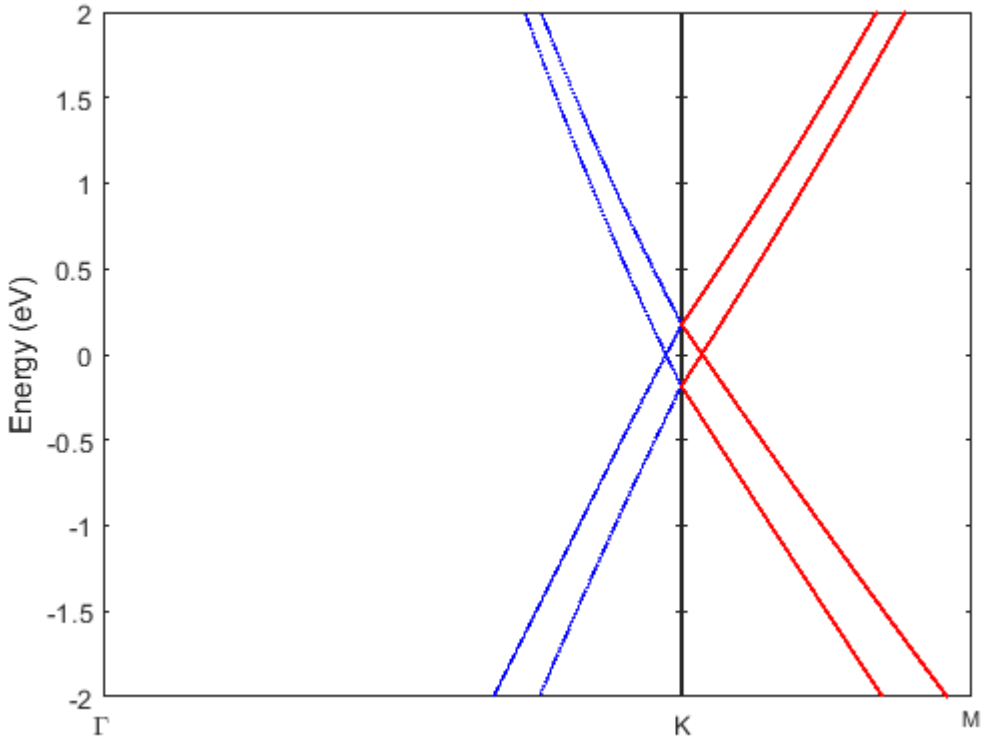

(b) $\Delta y = \frac{a}{10}$

Figure 3.5: Shift in the y direction in intervals of $\Delta y = \frac{a}{10}$ from 0 to a, corresponding to a shift from AA and back to AA configurations

Band splitting (eV)		
Shift	$\Gamma - K$	$K - M$
$0, 0$	0.000	0.000
$\frac{a}{10\sqrt{3}}, \frac{a}{10}$	0.083	0.045
$\frac{2a}{10\sqrt{3}}, \frac{2a}{10}$	0.086	0.047
$\frac{3a}{10\sqrt{3}}, \frac{3a}{10}$	0.108	0.066
$\frac{4a}{10\sqrt{3}}, \frac{4a}{10}$	0.083	0.065
$\frac{5a}{10\sqrt{3}}, \frac{5a}{10}$	0.000	0.000
$\frac{6a}{10\sqrt{3}}, \frac{6a}{10}$	0.000	0.065*
$\frac{7a}{10\sqrt{3}}, \frac{7a}{10}$	0.024	0.004*
$\frac{8a}{10\sqrt{3}}, \frac{8a}{10}$	0.000	0.000
$\frac{9a}{10\sqrt{3}}, \frac{9a}{10}$	0.000	0.000
$\frac{a}{\sqrt{3}}, a$	0.000	0.000

Table 3.3: Table of band splitting values for top layer shifts with respect to the bottom layer along the diagonal-direction

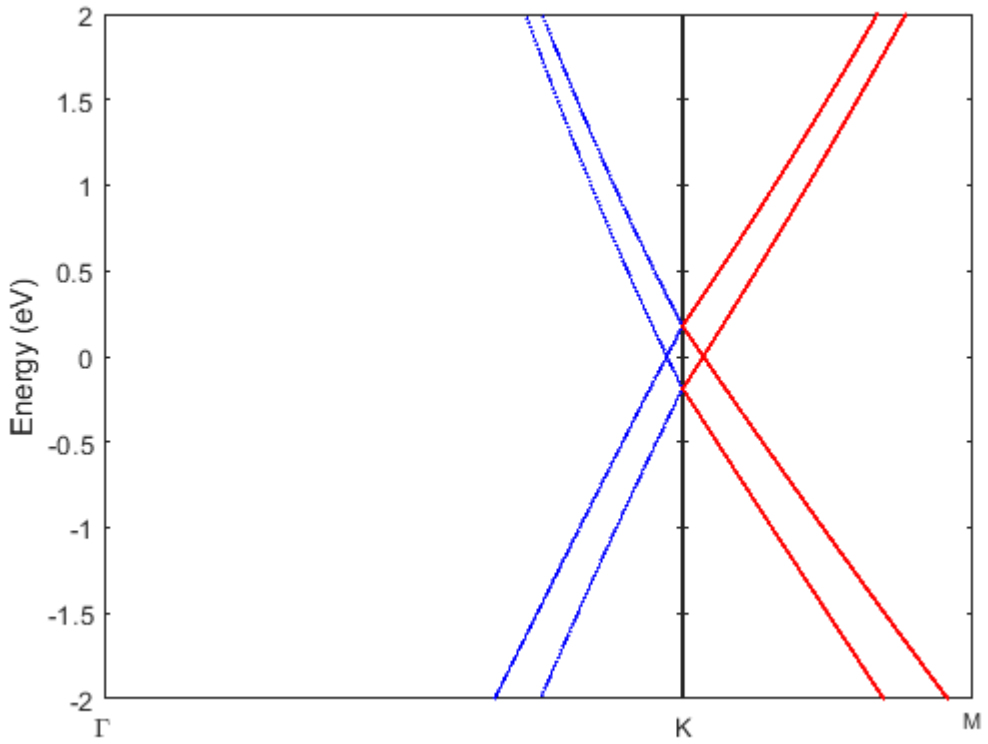

(a) $\Delta x = 0, \Delta y = 0$

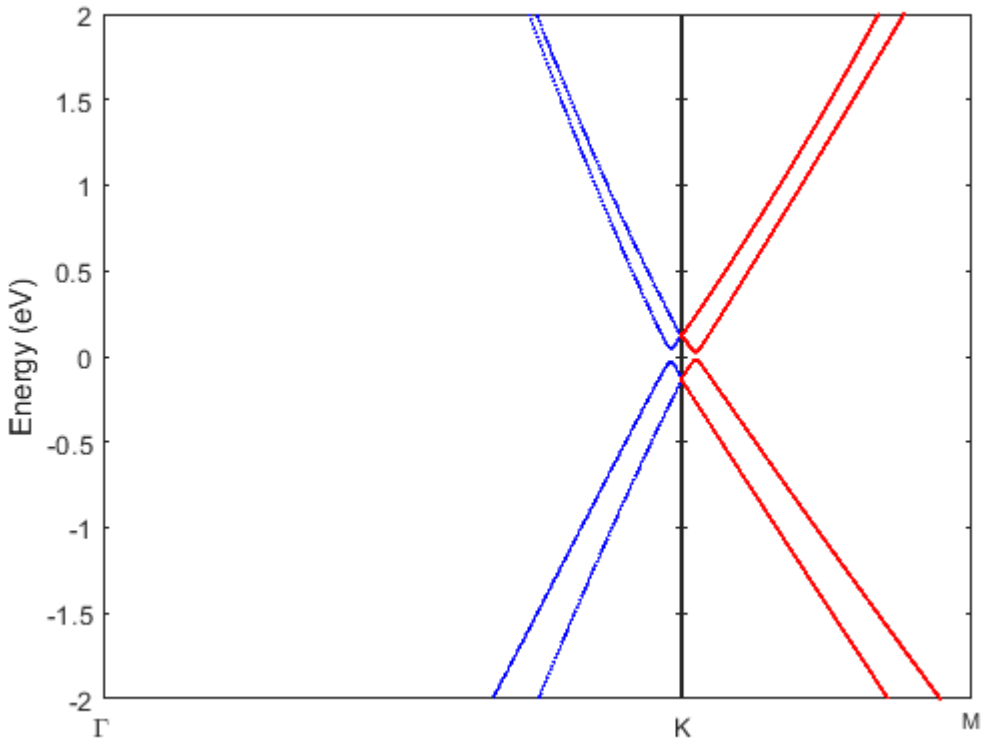

(b) $\Delta x = \frac{a}{10\sqrt{3}}, \Delta y = \frac{a}{10}$

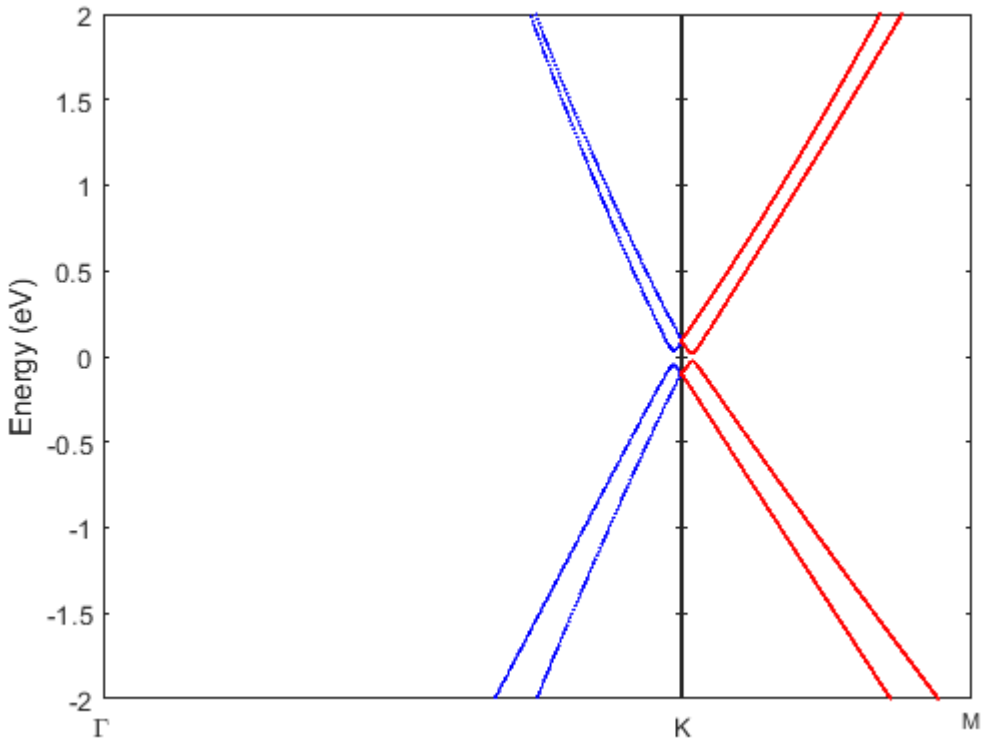

(c) $\Delta x = \frac{2a}{10\sqrt{3}}, \Delta y = \frac{2a}{10}$

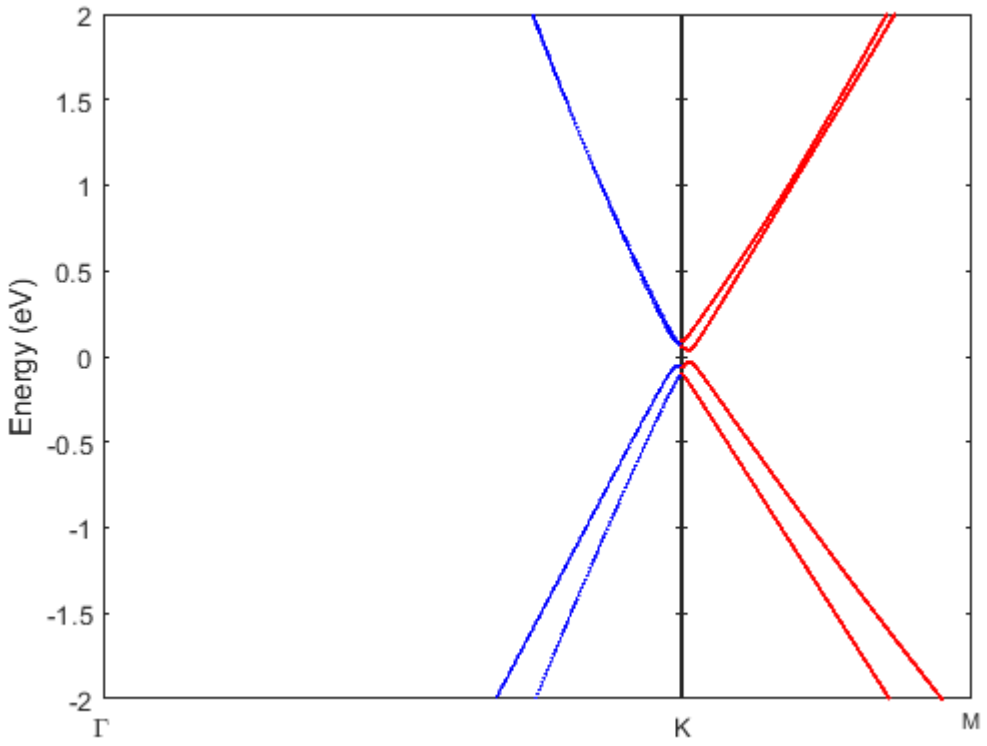

(a) $\Delta x = \frac{3a}{10\sqrt{3}}, \Delta y = \frac{3a}{10}$

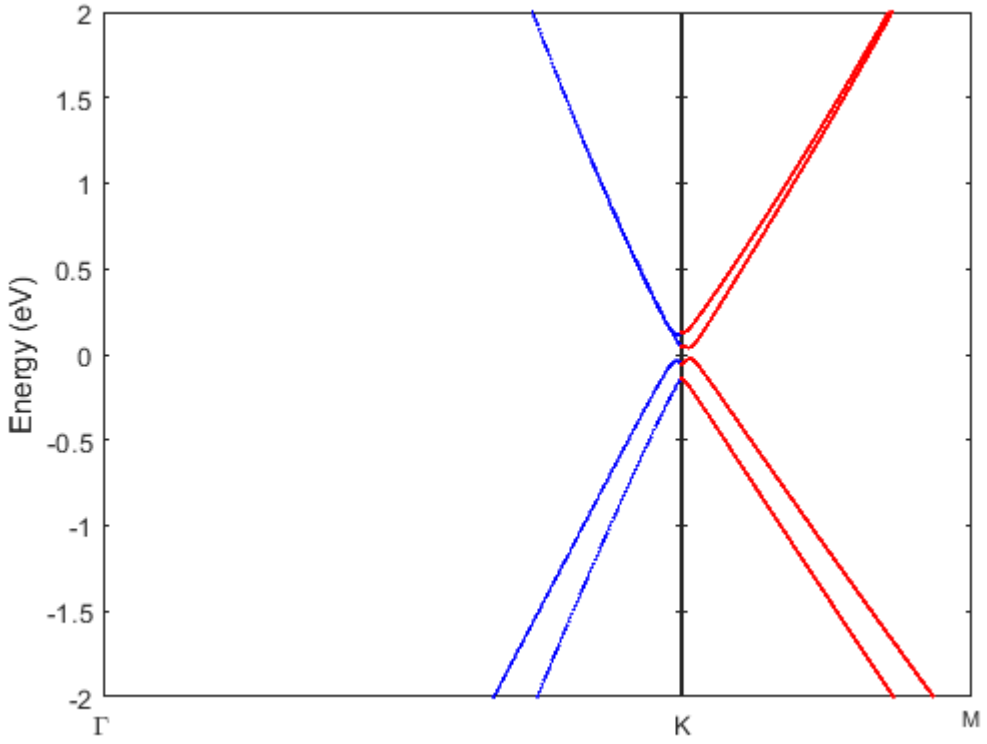

(b) $\Delta x = \frac{4a}{10\sqrt{3}}, \Delta y = \frac{4a}{10}$

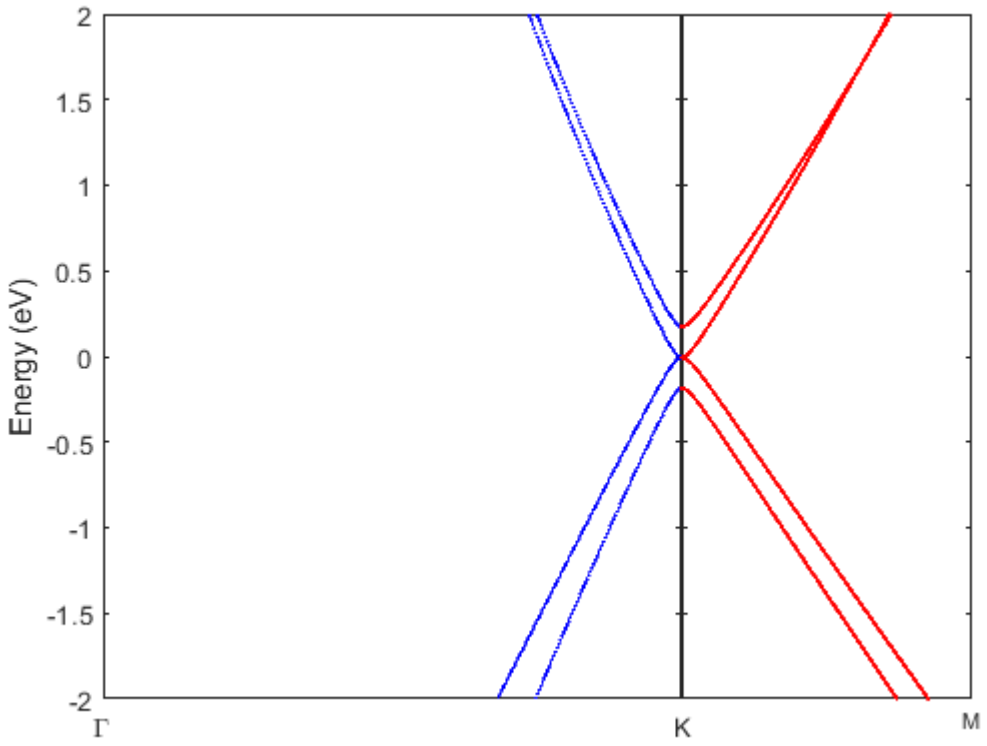

(c) $\Delta x = \frac{5a}{10\sqrt{3}}, \Delta y = \frac{5a}{10}$

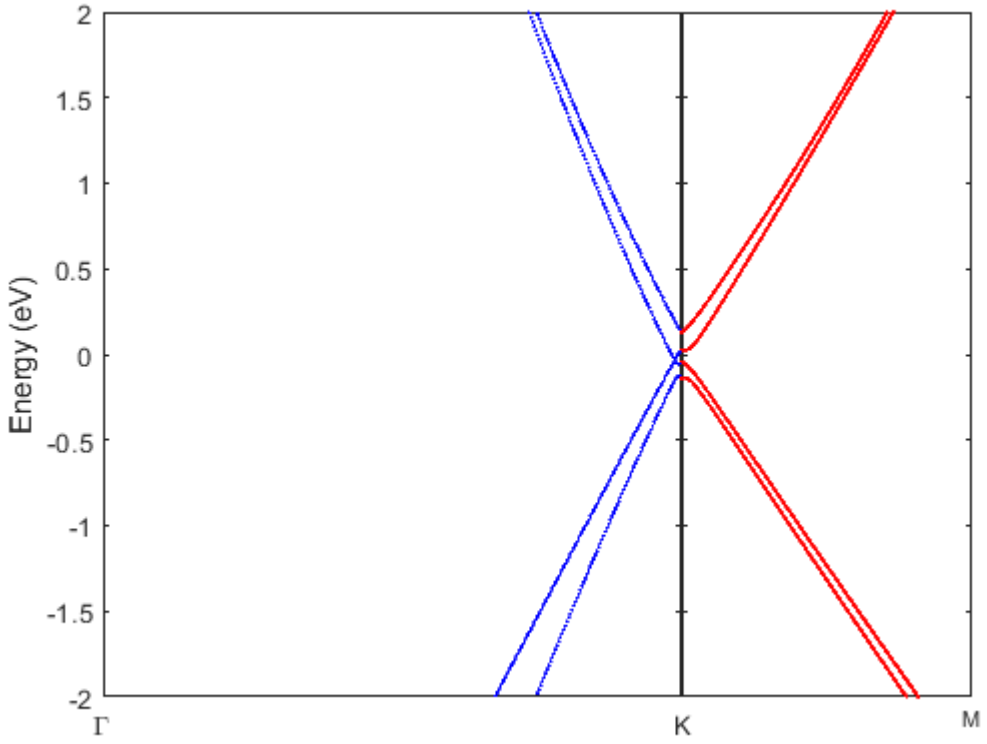

(d) $\Delta x = \frac{6a}{10\sqrt{3}}, \Delta y = \frac{6a}{10}$

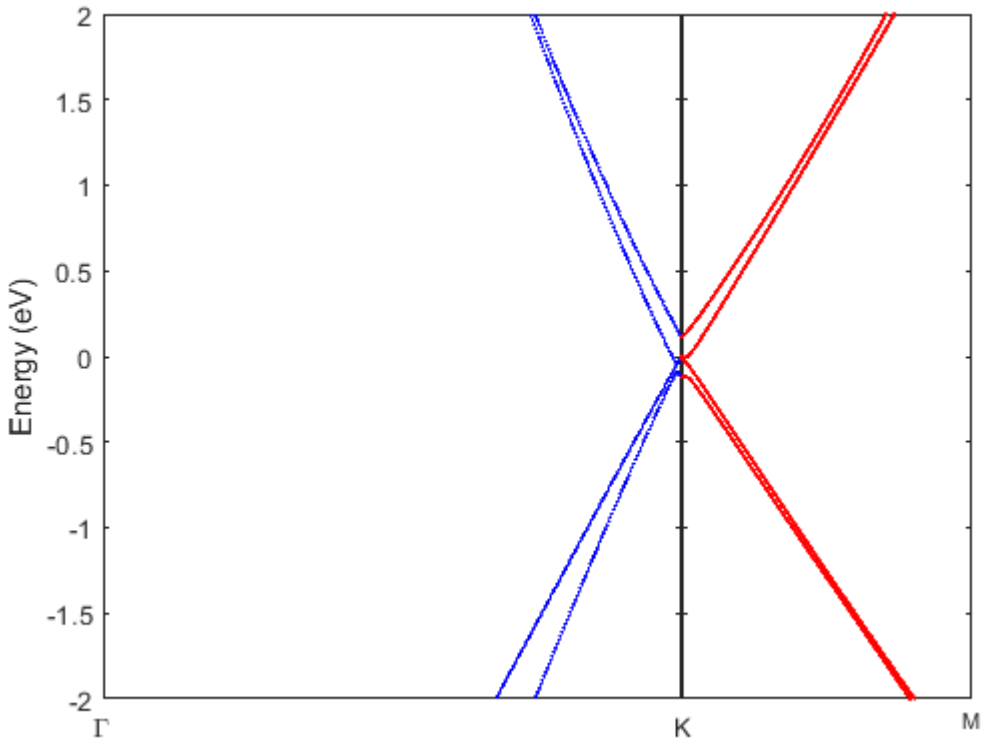

(a) $\Delta x = \frac{7a}{10\sqrt{3}}, \Delta y = \frac{7a}{10}$

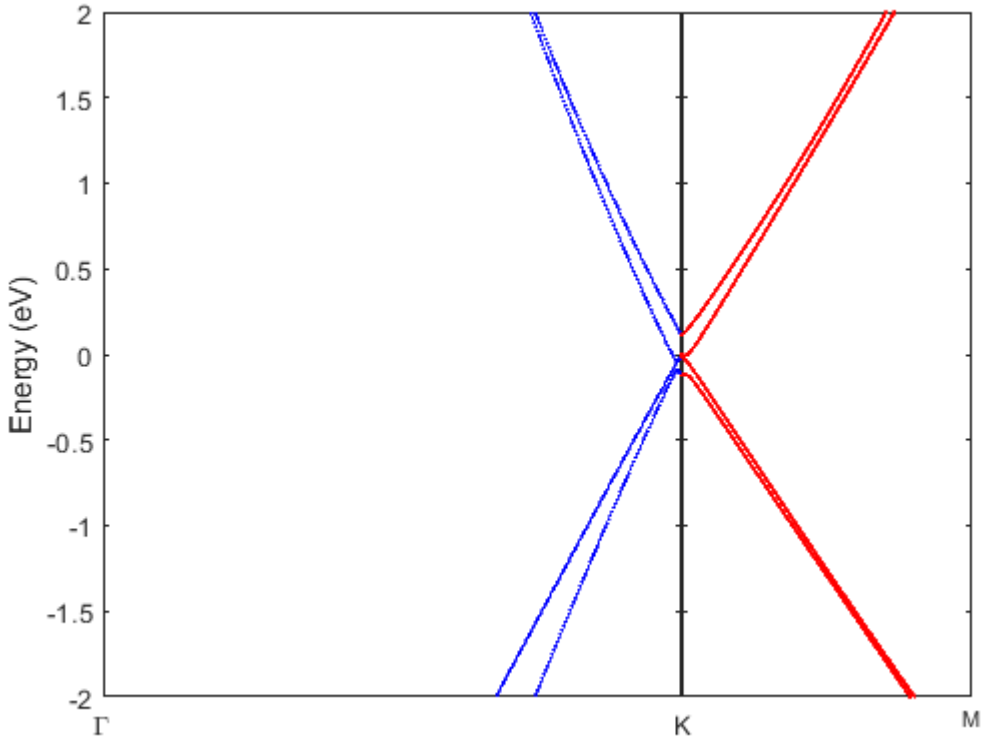

(b) $\Delta x = \frac{8a}{10\sqrt{3}}, \Delta y = \frac{8a}{10}$

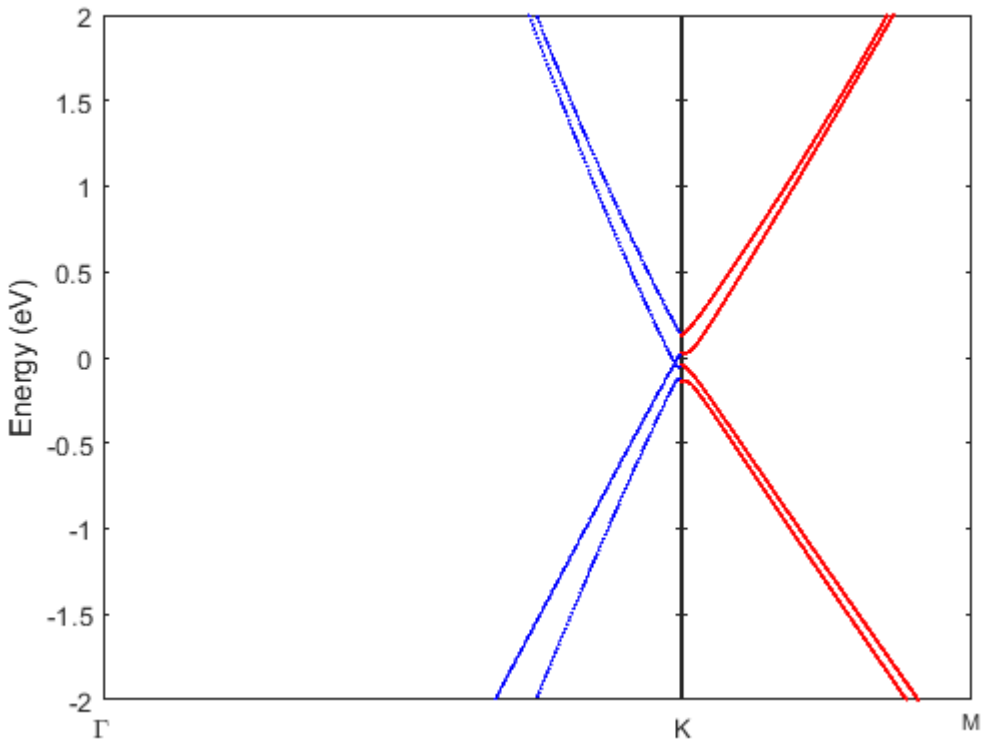

(c) $\Delta x = \frac{9a}{10\sqrt{3}}, \Delta y = \frac{9a}{10}$

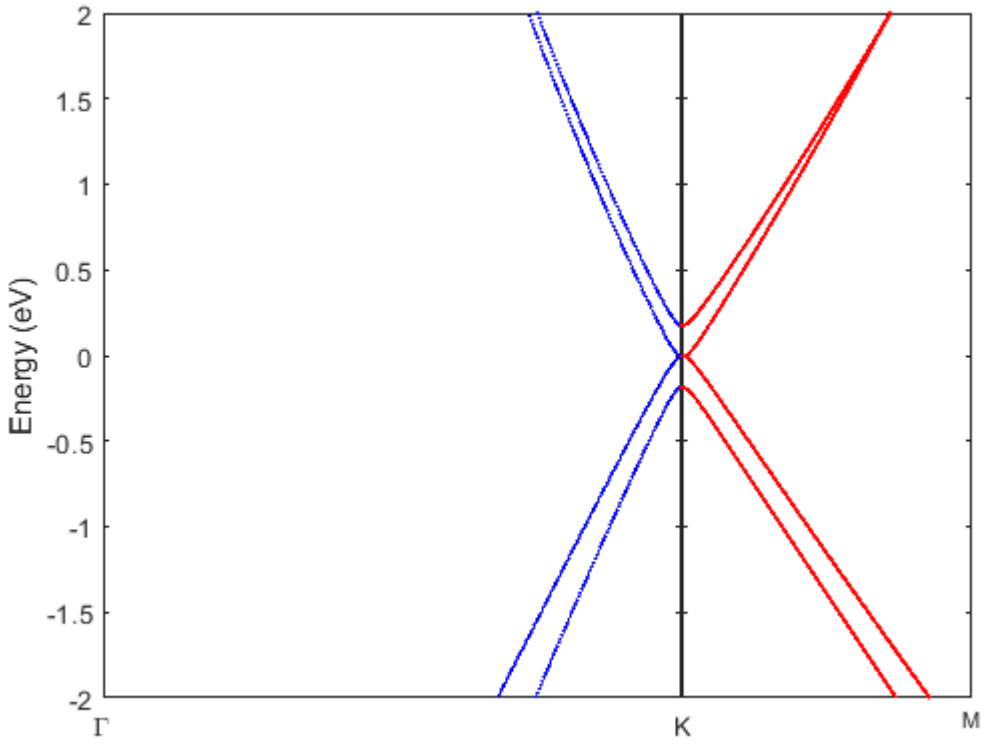

(d) $\Delta x = \frac{a}{\sqrt{3}}, \Delta y = a$

Figure 3.8: Shifts in the diagonal direction, in intervals of $\left(\frac{a}{10\sqrt{3}}, \frac{a}{10}\right)$ from $[0, 0]$ to $\left[\frac{a}{\sqrt{3}}, a\right]$, corresponding to a shift from AA to AB configurations

3.2 Loading Bilayer Graphene

We apply our tight binding parameter model to investigating the changes in the electronic band structure of bilayer graphene for a shift of the upper monolayer in a direction normal to the monolayer plane, i.e z-direction. The band structure of both AA and AB stackings approach the band structure of monolayer graphene as the vertical separation distance increases. This observation is necessary, but may not be sufficient for testing the usefulness of our tight binding parameter model. The z-shifts are done for intervals of $\frac{c}{10}$ over the range $\left[\frac{6c}{10}\frac{15c}{10}\right]$, where $c = 3.35\mathring{A}$ is the interlayer lattice parameter. where the signs indicate it's relative to the equilibrium distance, c.

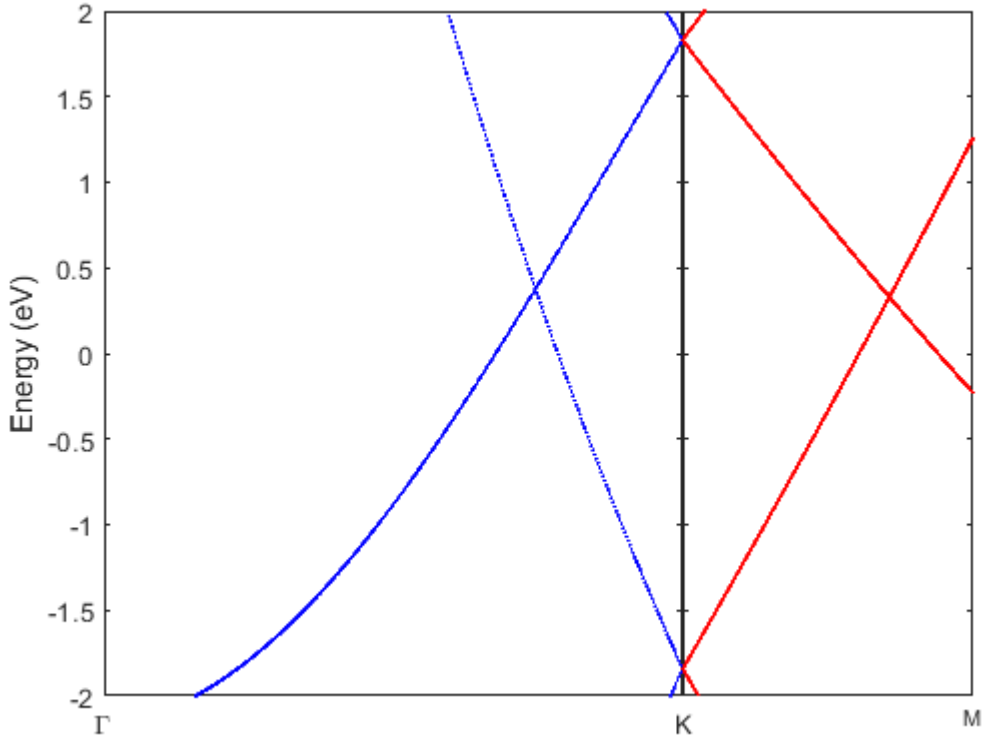

(a) $\Delta z = -\frac{4c}{10}$

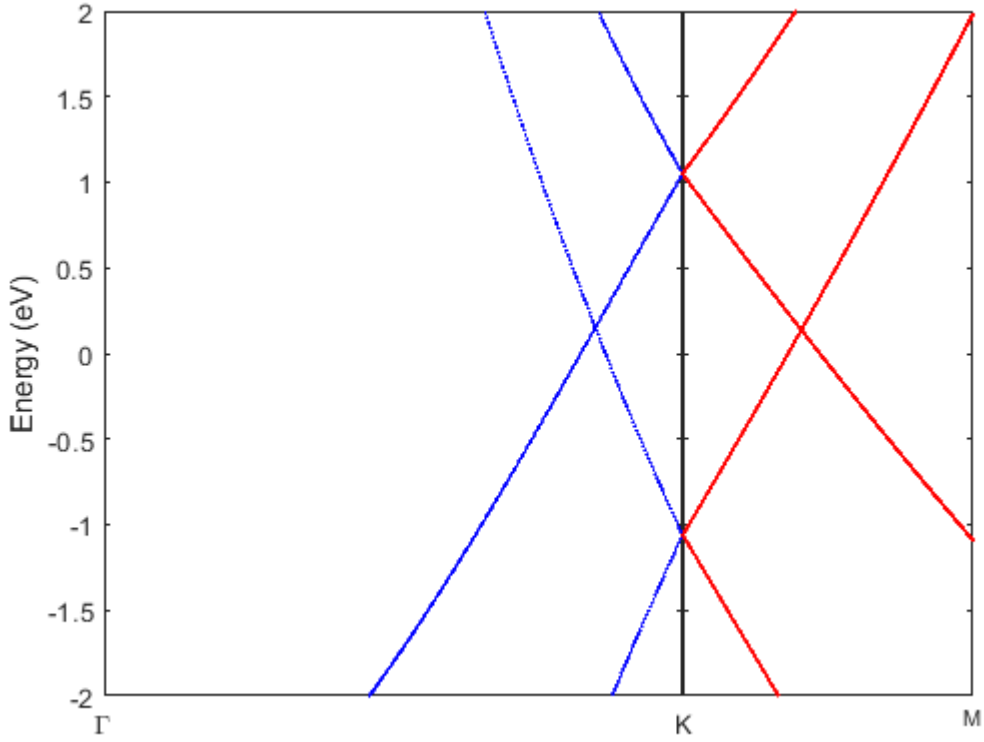

(b) $\Delta z = -\frac{3c}{10}$

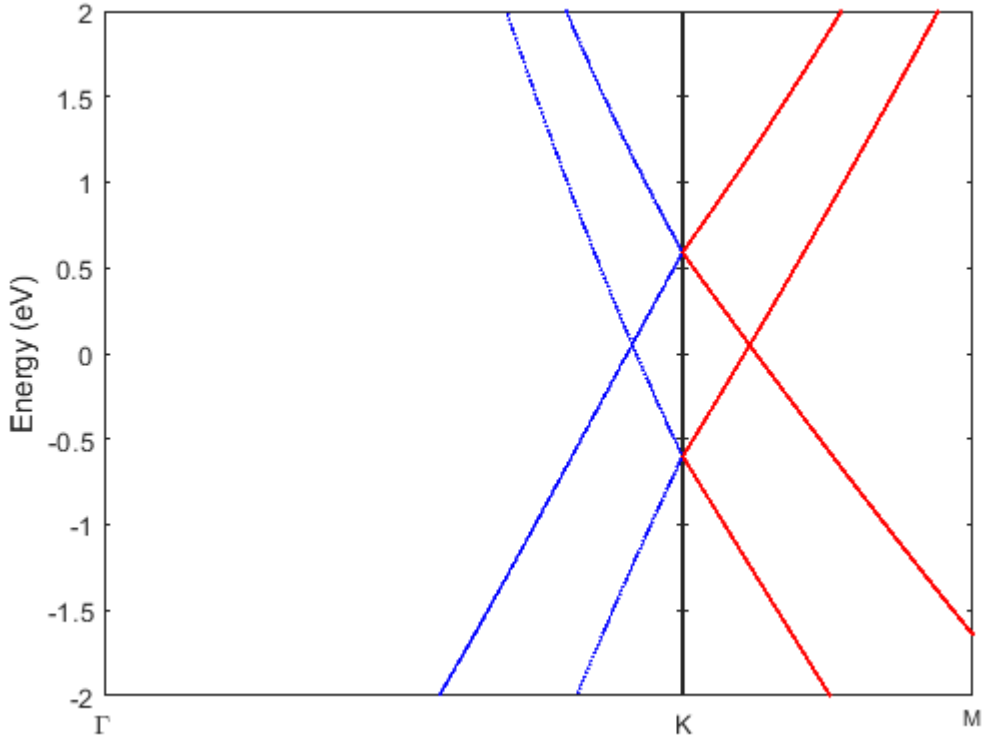

(c) $\Delta z = -\frac{2c}{10}$

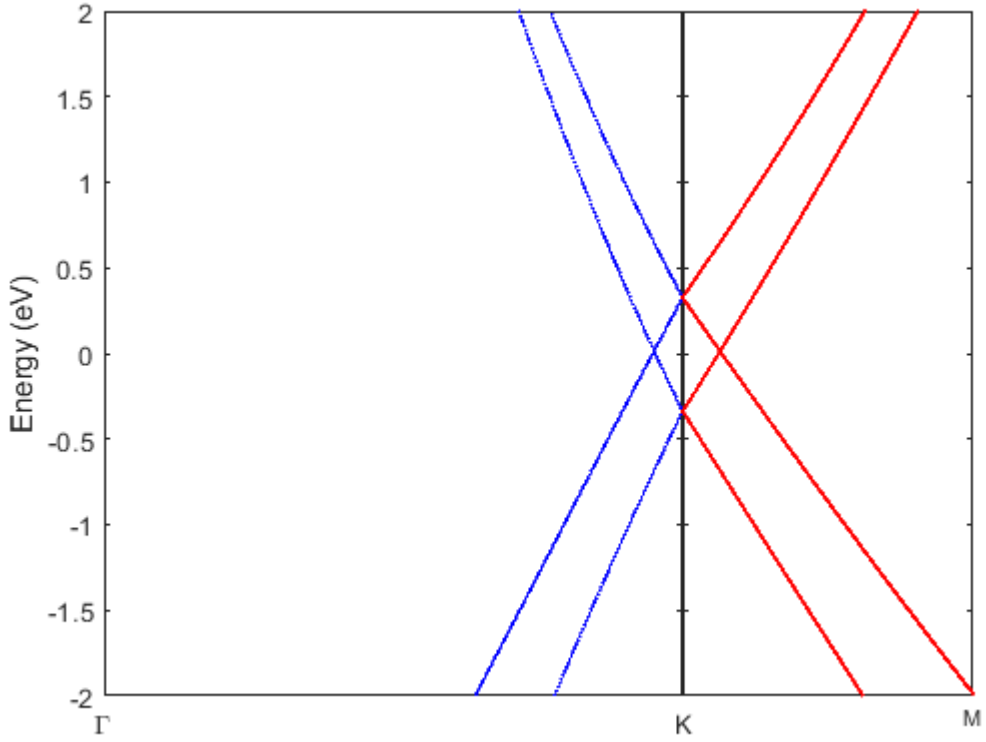

(d) $\Delta z = -\frac{c}{10}$

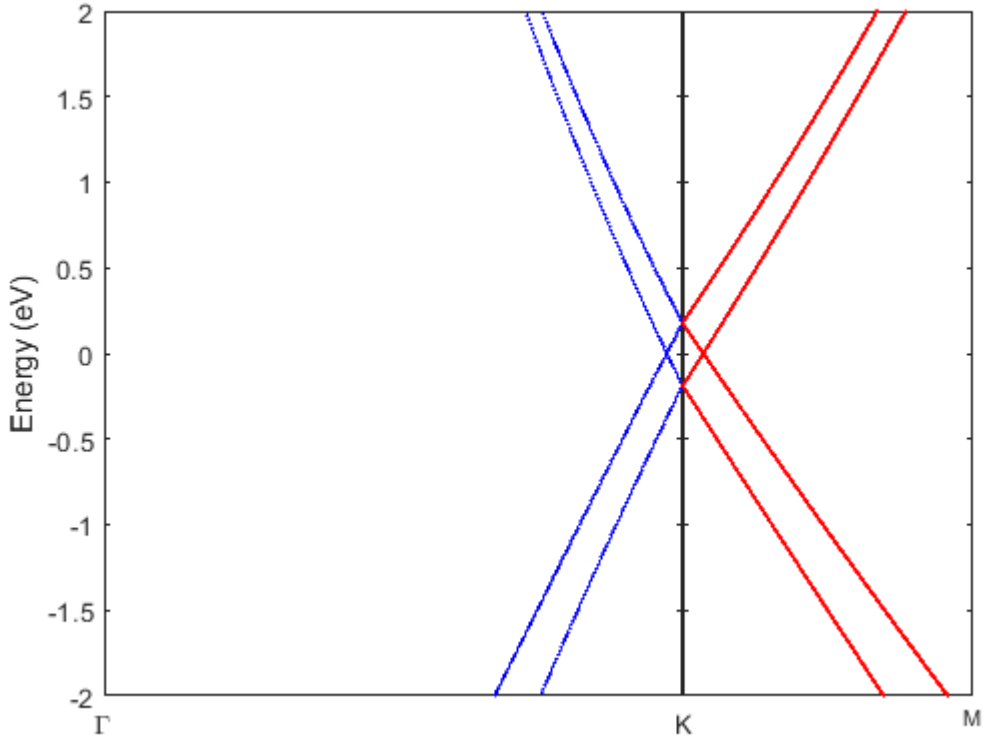

(e) $\Delta z = 0$

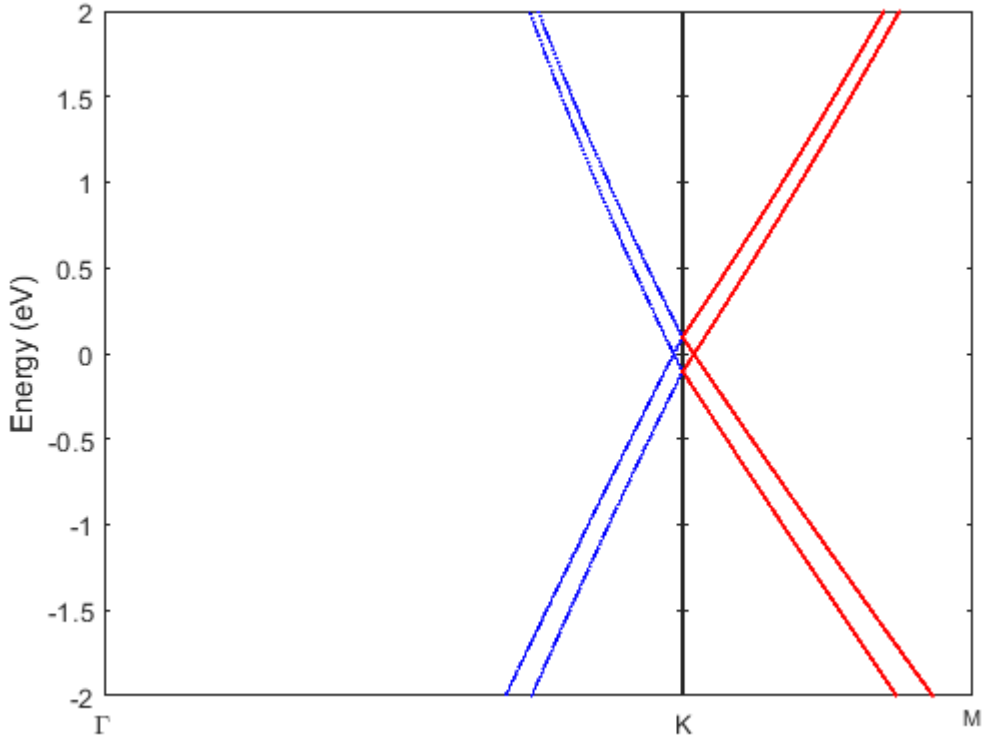

(f) $\Delta z = \frac{c}{10}$

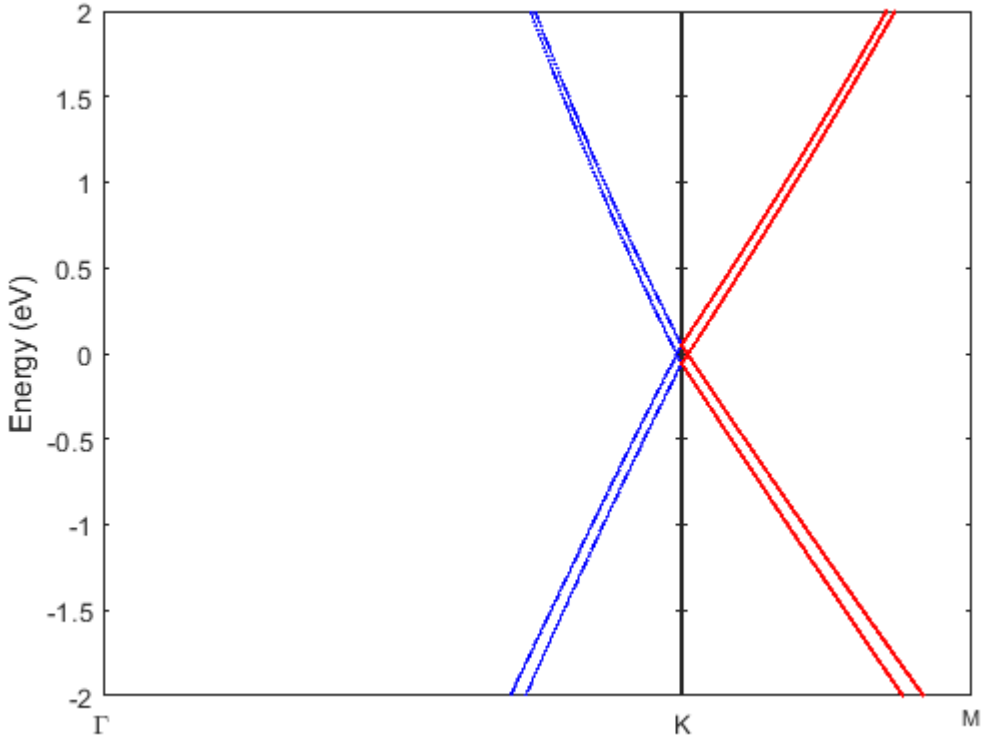

(g) $\Delta z = \frac{2c}{10}$

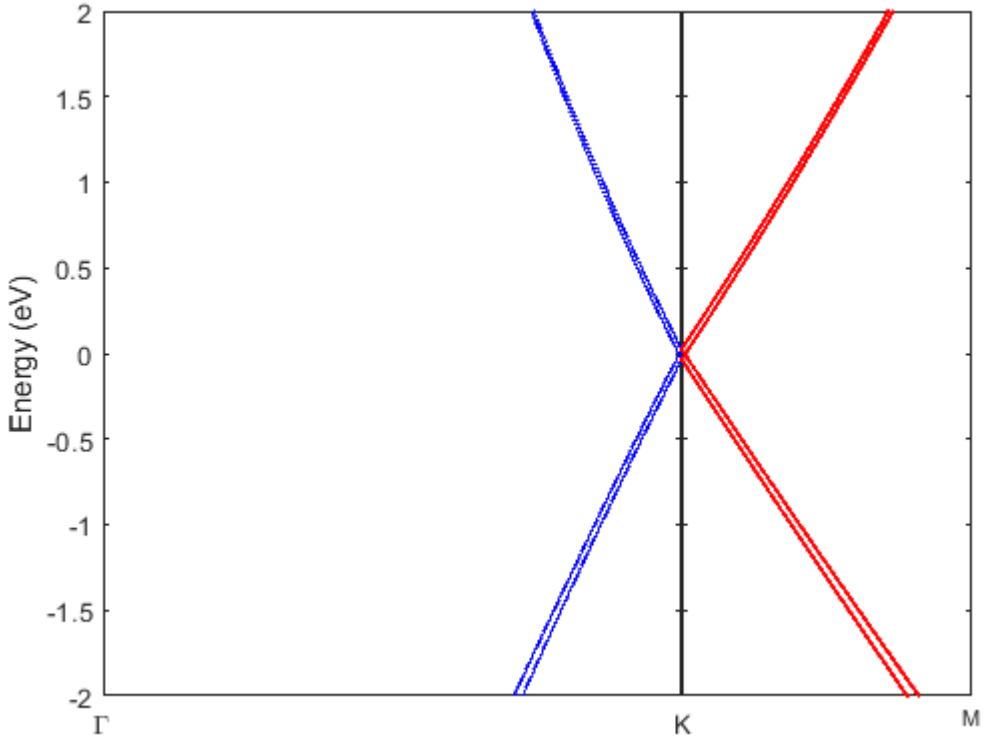

(h) $\Delta z = \frac{3c}{10}$

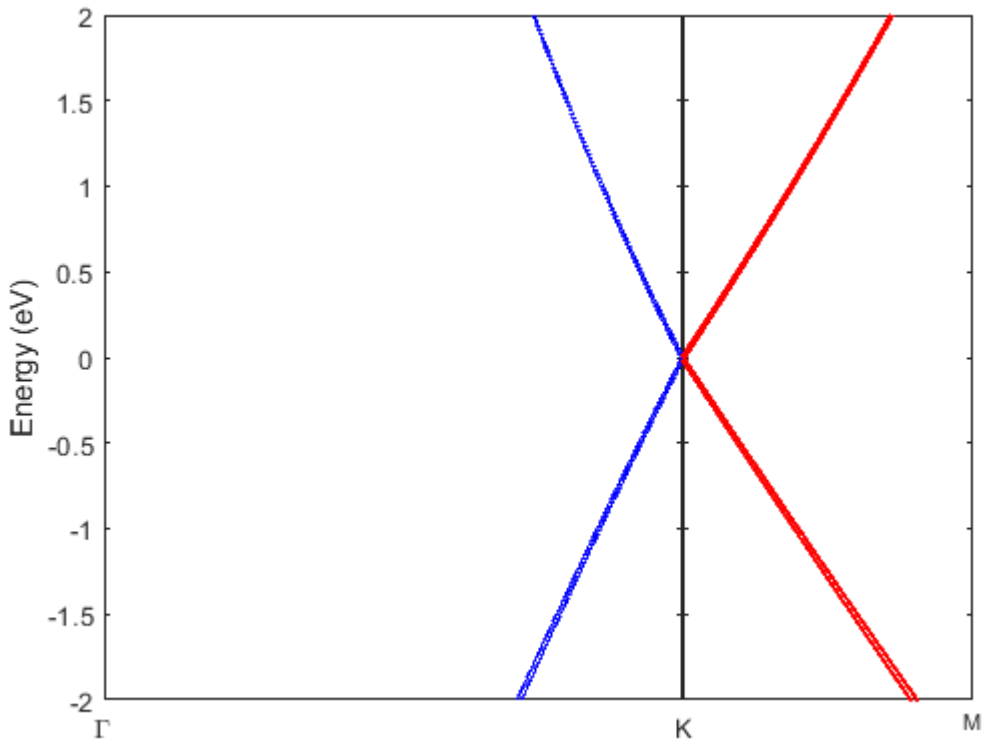

(i) $\Delta z = \frac{4c}{10}$

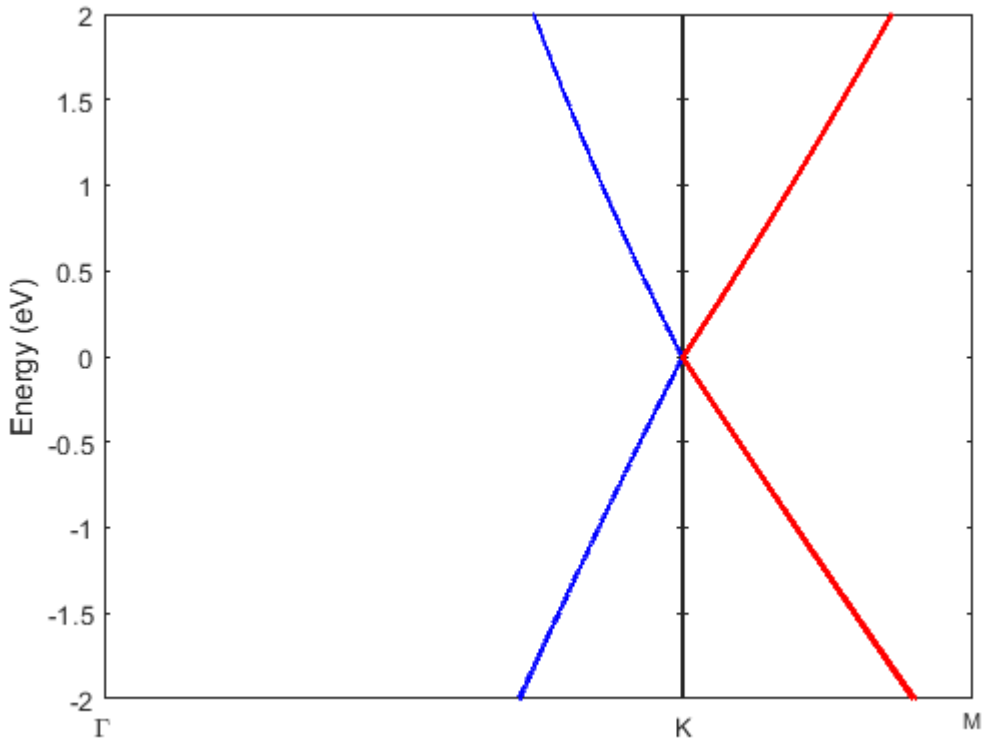

(j) $\Delta z = \frac{5c}{10}$

Figure 3.9: Varying interlayer distance, AA stacking configuration. Shown are band structures for increasing interlayer distance, from $z = \frac{6c}{10}$ to $z = \frac{15c}{10}$. Δz is the change in interlayer distance from the equilibrium separation, $c = 3.35\mathring{A}$

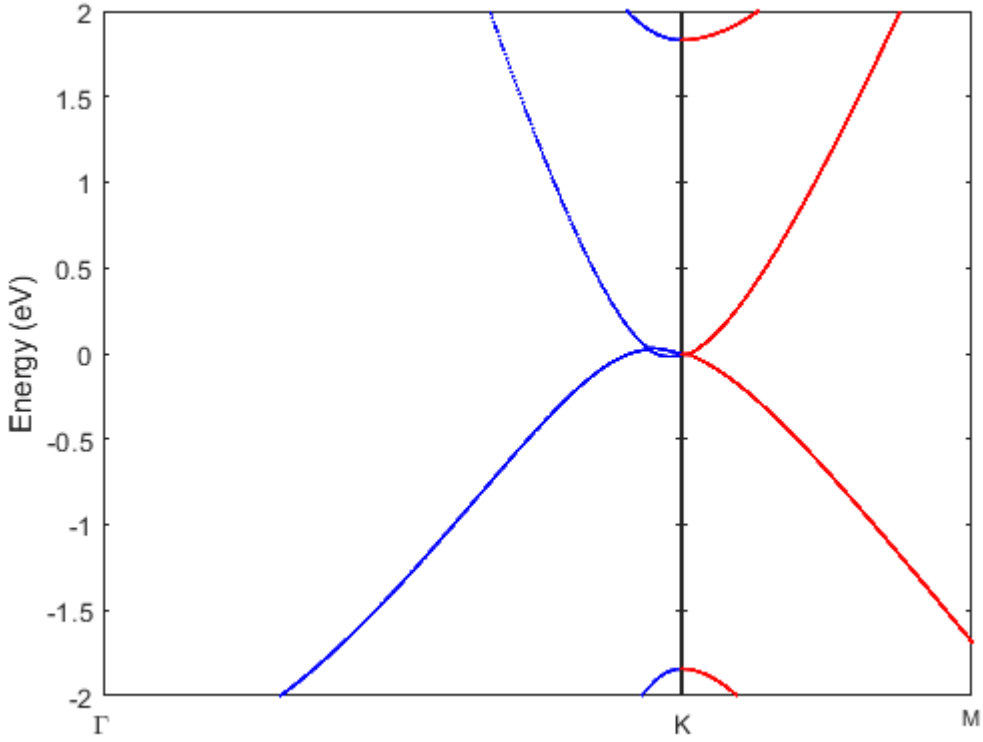

(a) $\Delta z = -\frac{4c}{10}$

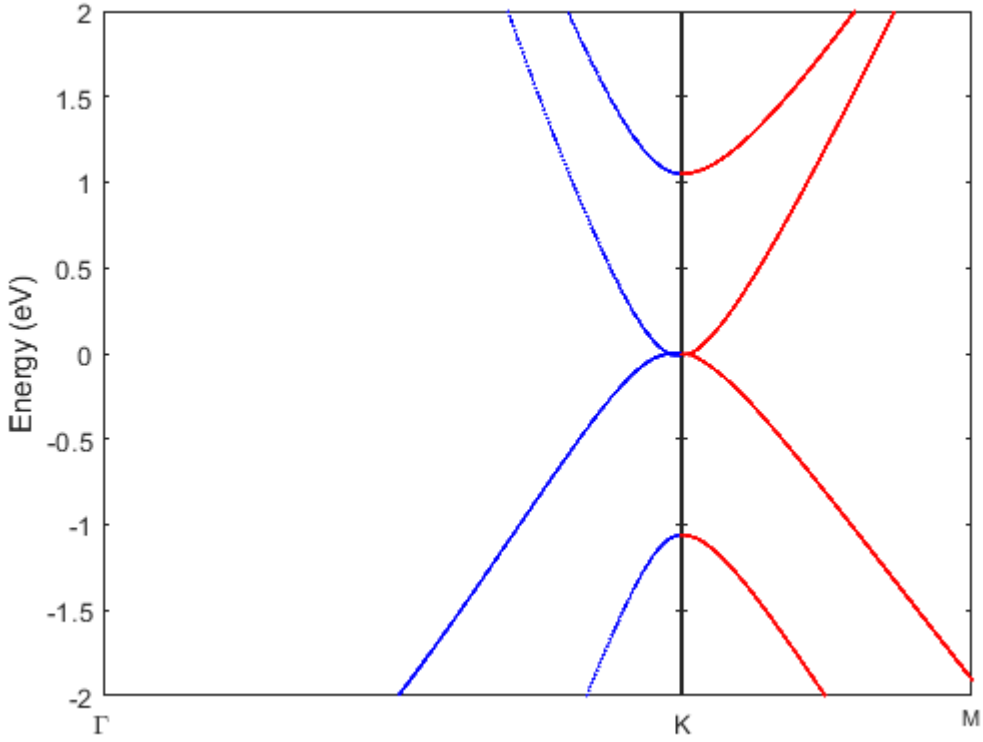

(b) $\Delta z = -\frac{3c}{10}$

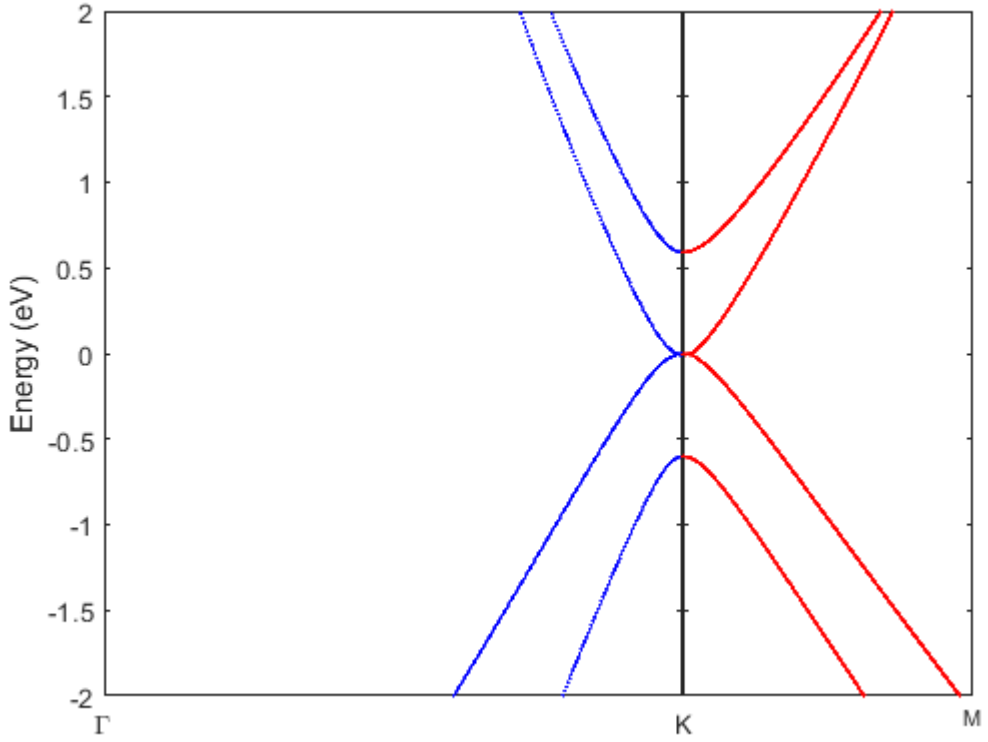

(c) $\Delta z = -\frac{2c}{10}$

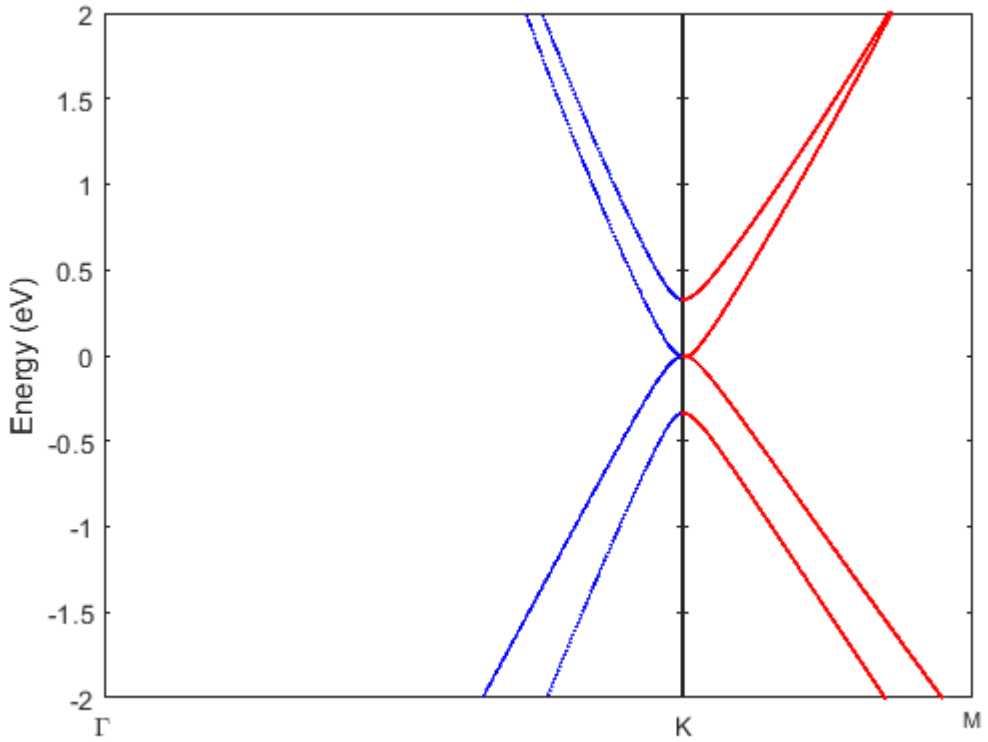

(d) $\Delta z = -\frac{c}{10}$

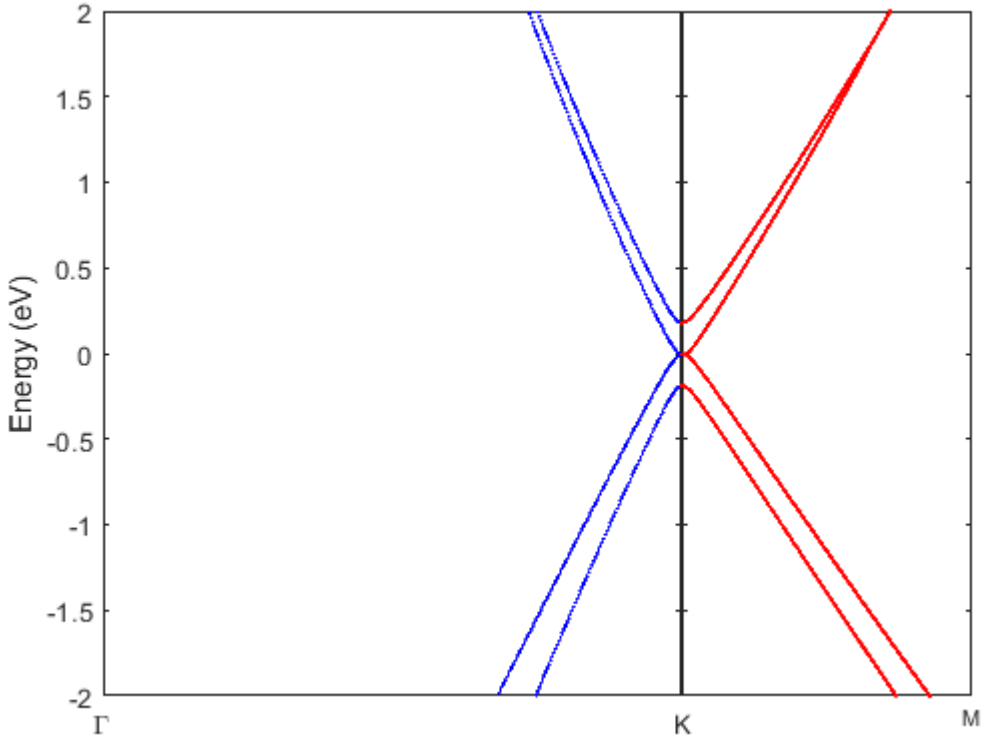

(e) $\Delta z = 0$

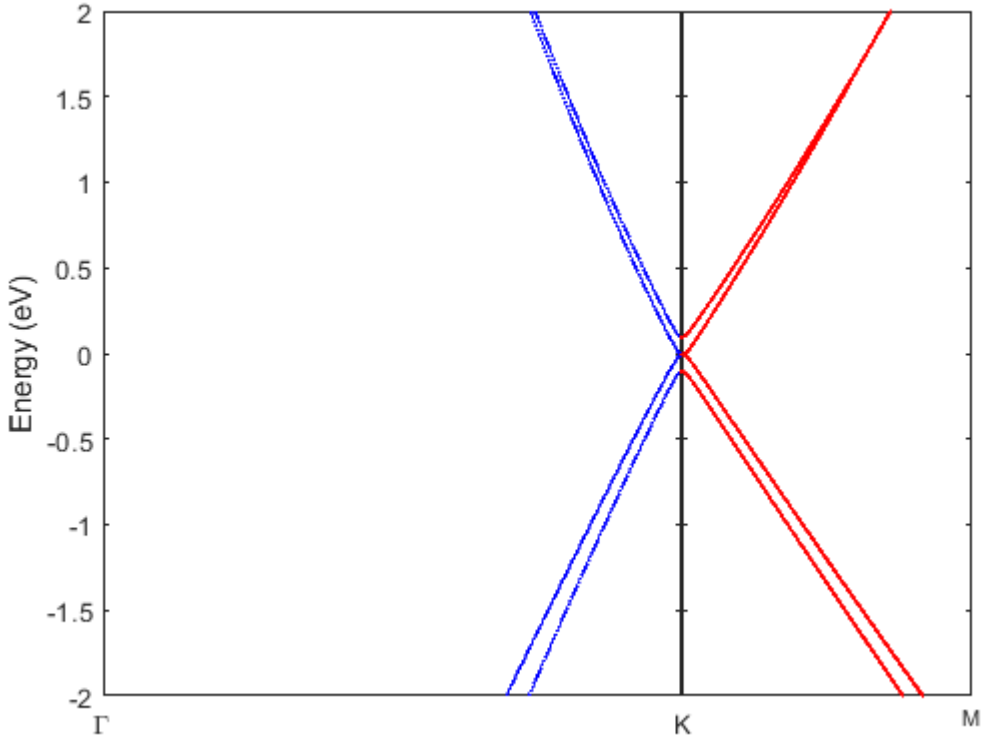

(f) $\Delta z = \frac{c}{10}$

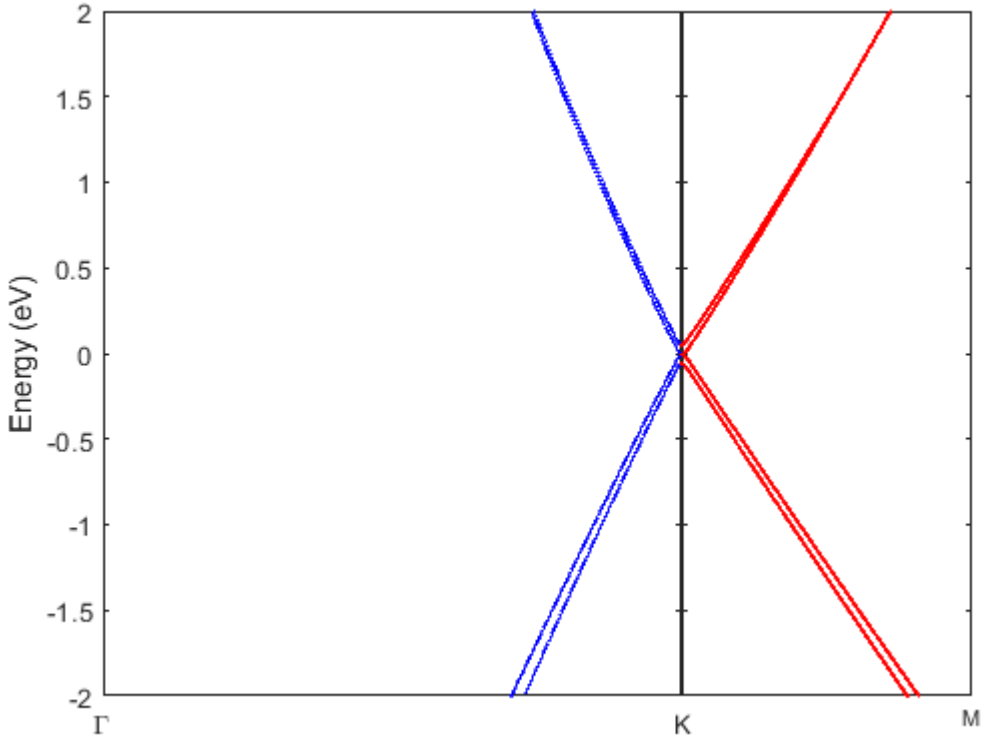

(g) $\Delta z = \frac{2c}{10}$

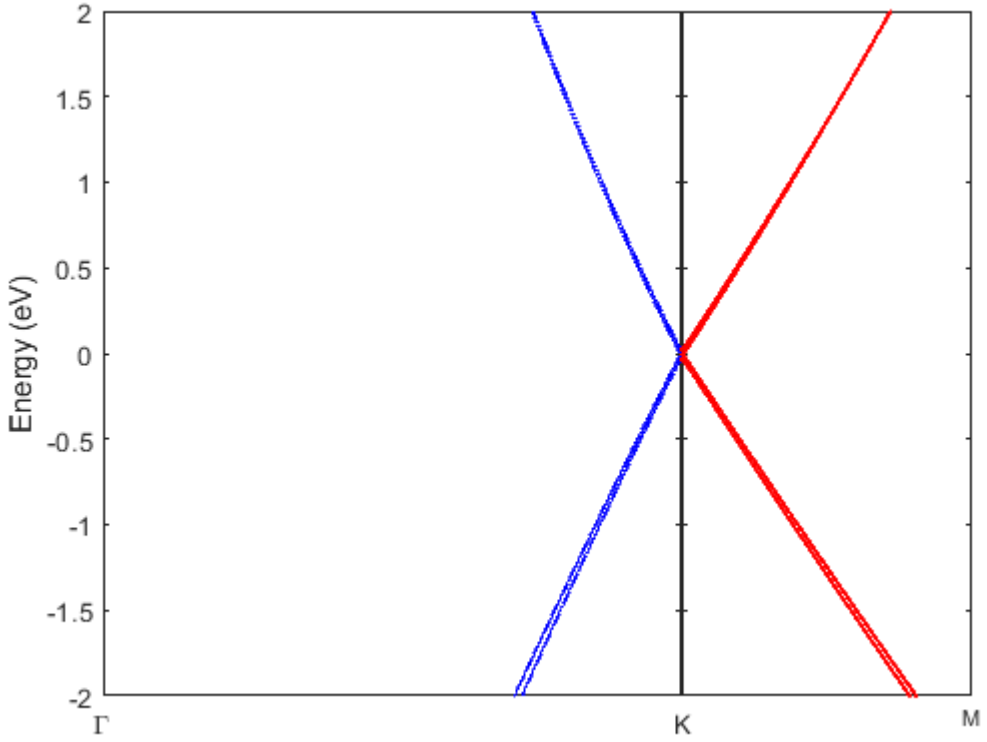

(h) $\Delta z = \frac{3c}{10}$

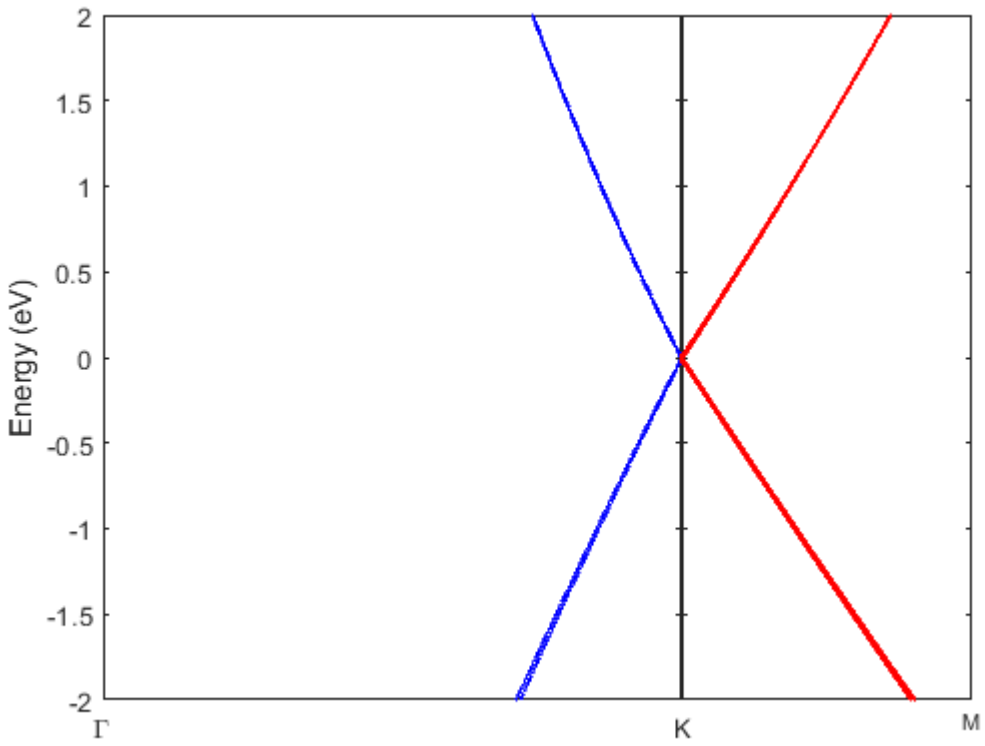

(i) $\Delta z = \frac{4c}{10}$

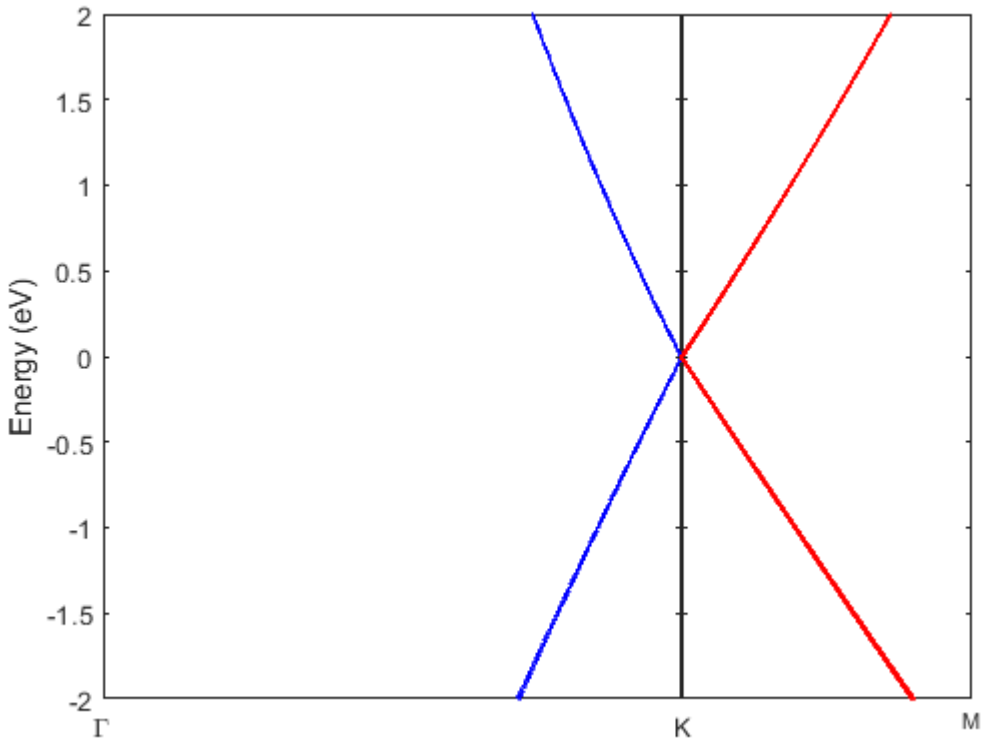

(j) $\Delta z = \frac{5c}{10}$

Figure 3.10: Varying separation distances, AB stacking. Shown are band structures for increasing monolayer separation distances, from $z = \frac{6c}{10}$ to $z = \frac{15c}{10}$. Δz is the change in interlayer distance from the equilibrium separation, $c = 3.35\mathring{A}$

Chapter 4

Effective Mass

The curvature $E(k)$ of the band structure of bilayer graphene, AB stacking, allows us to investigate its effective mass using the quadratic model

$$m = \hbar^2 \left(\frac{d^2 E}{dk^2} \right)^{-1} \tag{4.1}$$

We thus determine the effective mass of bilayer graphene and graphene, approximately by increasing the interlayer distance. Since our band structure approaches the band structure of monolayer graphene, which is linear in the neighborhood of the K point we expect that the quadratic model starts to fail significantly beyond an interlayer distance.

The $\Gamma - K$ and $K - M$ directions are fitted separately. Keeping in mind that the band structure becomes more linear away from the K point and that the structure of monolayer is linear in the region of the K points, we start fitting band structure $E - k$ values from the K point outward, and we keep adding points until the quadratic model starts to fail significantly. On average including $E - k$ values at the K points we fitted an average of five $E - k$ values.

Fig. 4.1 shows the variation of effective mass with separation distance for different bands. We focus on the lower lying bands. For both the valence and conduction bands, effective mass reduces with increasing separation until it reaches a minimum and starts to increase again. Normally we would expect that an increase in separation distance should result in a reduction in the overlap of orbitals and

thus an increase in effective mass. So why do we see a decrease here? The band structure bilayer graphene can viewed as a perturbation of the band structure of monolayer graphene. So that effectively the change that matters is the change in in-plane p_z orbital interactions. The smaller the p_z-orbital overlap out-of -plane, the bigger the p_z orbital overlap in-plane, and the smaller the effective mass. Using a spline fit, the lower energy conduction band has a mimimum effective mass of approximately $0.018m_e$ at an interlayer distance of $4.41 \times 10^{-10}m$, for the effective mass of electrons in monolayer graphene, and the lower energy valence band, a mimimum effective mass of approximately $0.021m_e$ at about the same interlayer distance. These values are comparable to $m_e^* = 0.012m_e$ reported in [23]. The effective mass of electrons (fermi level conduction band) and holes (fermi level valence band), $m_e^* = 0.030m_e$ and $m_h^* = 0.034m_e$ are similar to the values $m_e^* = 0.041m_e$ and $m_h^* = 0.036m_e$ reported in [24]. Also effective mass values for 2NN in-plane interactions are $m_e^* = 0.032m_e$ and $m_h^* = 0.045m_e$ respectively. The results obtained for 2NN and 4NN in-plane and out-of-plane interactions seem to suggest that the number of nearest neighbour interactions considered may affect the accuracy/predictive power of tight-binding parameter functions. The band structure in the $K - M$ direction is almost horizontal, close to the K point over the first three vertical shifts beyond the equilibrium distance. This is not observed in 2NN interactions, as the energy follows a quadratic model over these shifts. Also as previously mentioned the linearity of the band structure as it approaches a monolayer limit ensures that the quadratic modeling of the energy graph fails, hence the increase in the effective mass with increasing separation distance after the minimum.

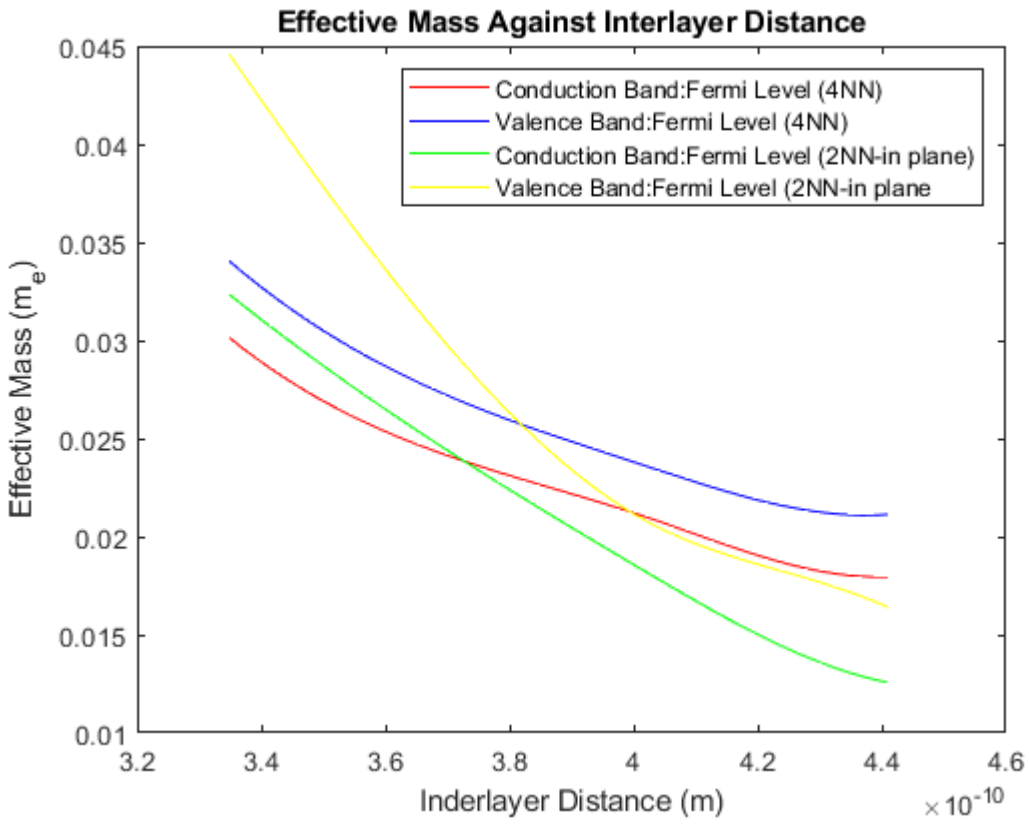

Figure 4.1: Effective mass against interlayer distance

Chapter 5

Conclusion

In this thesis we made tight binding parameters into functions of interacting distance. In Chapter 2 we discussed the tight binding model, as applied to calculating the band structure of monolayer and bilayer graphene for at most 1NN interactions in-plane and 2NN interactions out-of-plane.In Chapter 3 after developing the tight binding parameter functions we apply these functions to the calculation of the band structure of bilayer graphene sliding in three different directions, and observed band splittings, which showed patterns for some sliding directions. We also applied the tight binding parameter functions to bilayer graphene with varying interlayer distance for both the AA and AB stacking configurations, and show that our band structure approaches the monolayer limit in both configurations. In Chapter 5, we calculate the effective mass of electrons and holes in bilayer graphene for varying separation distance discussed in the previous chapter. We assume a quadratic energy dependence, and explain the pattern of change of the effective mass with changing separation distance. By this we determine approximately the effective mass of electrons in bilayer graphene, and the effective mass of electrons in monolayer graphene and compare our results to experimental results in literature, to this effect we find our theoretical results reasonable and thus the model useful. We also realize that although a quadratic fit works for both $\Gamma - K$ and $K - M$ directions for in-plane interactions of 2NN, only the $\Gamma - K$ direction can be reasonably fitted for effective mass calculations

for 4NN interactions. The slope of the band line in the $K - M$ direction close the K point is horizontal for corresponding quadratic dependence of energy in the $\Gamma - K$ direction, which maybe a suggestion of masslessness in that region. We also would like to suggest that tight-binding parameter functions may be limited by the number of nearest neighbour interactions.

Bibliography

[1] H. Min, B. Sahu, S. K. Barnejee, and A. H. MacDonald, "Ab initio theory of gate induced gaps in graphene bilayers," *Physical Review Letters*, vol. 75, no. 155115, 2007.

[2] S. Latil and L. Henrard, "Charge carriers in few-layer graphene films," *Physical Review Letters*, vol. 97, no. 036803, 2006.

[3] S. B. Trickey, F. Muller-Plathe, G. H. F. Diercksen, and J. C. Boettger, "Interplanar binding and lattice relaxation in a graphite dilayer," *Physical Review B*, vol. 45, no. 8, 1992.

[4] M. Dresselhaus and G. Dresselhaus, "Intercalation compounds of graphite," *Advances in Physics*, vol. 51, no. 1, pp. 1 – 186, 2002.

[5] C. M. Cheng, C. J. Hsu, J. L. Peng, C. H. Chen, J. Y. Yuh, and K. D. Tsuei, "Tight-binding parameters of graphite determined with angle-resolved photoemission spectra," *IEEE Transactions on Medical Imaging*, vol. 354, pp. 229 – 234, 2015.

[6] T. Filleter, J. L. McChesney, A. Bostwick, E. Rotenberg, K. V. E. T. Seyller, K. Horn, and R. Bennewitz, "Friction and dissipation in epitaxial graphene films," *Physical Review Letters*, vol. 102, no. 8, p. 086102, 2009.

[7] P. R. Wallace, "Band theory of graphite," *Physical Review*, vol. 71, no. 9, pp. 622 – 634, 1947.

[8] D. P. DiVincenzo and E. J. Mele, "Self-consistent effective-mass theory for intralayer screening in graphite intercalation compounds," *Physical Review B*, vol. 29, no. 4, pp. 1685 – 1694, 1984.

[9] K. S. Novoselov, A. K. Geim, S. V. Morozov, D. eng Jiang, Y. Zhang, S. V. Dubonos, I. V. Grigorieva, and A. A. Firsov, "Electric field effect in atomically thin carbon films," *Science*, vol. 306, pp. 666 – 669, 2004.

[10] Y. Zhang, T. T. Tang, C. Girit, Z. Hao, M. C. Martin, A. Zettl, M. F. Crommie, Y. R. Shen, and F. Wang, "Direct observation of a widely tunable bandgap in bilayer graphene," *Nature*, vol. 459, pp. 820–823, 2009.

[11] E. J. Kan, Z. Li, J. Yang, and J. G. Hou, "Will zigzag graphene nanoribbon turn to half metal under electric field?," *Applied Physics Letters*, vol. 91, 2007.

[12] F. J. Owens, "Electronic and magnetic properties of armchair and zigzag graphene nanoribbons," *Journal of Chemical Physics*, vol. 128, 2008.

[13] H. Ren, Q. X. Li, Y. Luo, and J. Yang, "Graphene nanoribbon as a negative differential resistance device," *Applied Physics Letters*, vol. 94, 2009.

[14] B. Xu, J. Yin, Y. D. Xia, X. G. Wan, K. Jiarig, and Z. G. Liu, "Electronic and magnetic properties of zigzag graphene nanoribbon with one edge saturated," *Applied Physics Letters*, vol. 96, 2010.

[15] J. E. Fischer and A. T. Johnson, "Electronic properties of carbon nanotubes," *Current Opinion in Solid State and Materials Science*, vol. 4, pp. 28–33, 1999.

[16] T. Ando, "The electronic properties of graphene and carbon nanotubes," *NPG Asia Materials*, vol. 1, pp. 17–20, 2009.

[17] Y. Cao, V. Fatemi, S. Fang, K. Watanabe, T. Taniguchi, E. Kaxiras, and P. Jarillo-Herrero, "Unconventional superconductivity in magic-angle graphene superlattices," *Nature*, vol. 556, pp. 43–50, 2018.

[18] E. Kaxiras, *The electronic properties of graphene and carbon nanotubes*. New York: Cambridge University Press, 2003.

[19] B. Gharekhanlou and S. Khorasani, *An overview of tight-binding method for two-dimensional carbon structures, Graphene: Properties, Synthesis and Application.* Nova Science Publishers, 2011.

[20] P. Moon and M. Koshino, "Optical absorption twisted bilaye graphene," *Physical Review B*, vol. 87, no. 205404, pp. 1–10, 2013.

[21] M. Koshino, "Interlayer interaction in general incommensurate atomic layers," *New Journal of Physics*, vol. 17, no. 1, pp. 1–10, 2015.

[22] R. Kunda, "Tight-binding parameters for graphene," *Modern physics Letters*, vol. 25, no. 3, pp. 163–173, 2010.

[23] E. Tiras, S. Ardali, T. Tiras, E. Arslan, S. Cakmakyapan, O. Kazar, J. Hassan, E. Janzén, and E. Ozbay, "Effective mass of electron in monolayer graphene: Electron-phonon interaction," *Journal of Applied Physics*, vol. 84, no. 043708, 2013.

[24] K. Zou, X. Hong, and J. Zhu, "Effective mass of electrons and holes in bilayer graphene: Electron-hole asymmetry and electron-electron interaction," *Physical Review B*, vol. 84, no. 085408, 2011.